FAILURE BEHAVIOR OF LAMINATED COMPOSITES UNDER ANTICLASTIC BENDING

by

YAKUP OKAN ALPAY

B.S., Mechanical Engineering, Istanbul University, 2010

Submitted to the Institute for Graduate Studies in
Science and Engineering in partial fulfillment of
the requirements for the degree of
Master of Science

Graduate Program in Mechanical Engineering

Boğaziçi University

2014

ACKNOWLEDGEMENTS

First, I would like to express my sincere gratitude to my advisors Prof. Fazıl Önder Sönmez and Assoc. Prof. Nuri Ersoy for their patience and invaluable helps during my thesis study. I am also grateful to Kenan Çınar for his all support and practical solutions for the challenges I faced in my thesis studies. Special thanks to Murat Koç for his guidance. I would like to thank Niyazi Tanlak for all his encouragements

And...

Many thanks to Emel Türker who is always respectful to my studies and to my parents not for a particular reason but for everything all they have done for me.

ABSTRACT

FAILURE BEHAVIOR OF THE LAMINATED COMPOSITE PLATES UNDER ANTICLASTIC BENDING

In this study, failure behavior of laminated composite plates subjected to anti-clastic bending is investigated. Anticlastic bending is a special case of bi-axial out-of-plane loading that applies predominantly twisting moment. A unique test fixture is designed to achieve anticlastic loading condition. Totally nine different configurations are chosen and four specimens are tested for each configuration. Reinforcing strips are bonded to the edges of the specimens to reduce the delamination risk at the edges. Acoustic emission monitoring (AEM) is utilized to detect the first-ply-failure load. In this method, sounds resulting from initiation and progression of damage within the material are detected, then the signal data are processes to identify the failure modes and determine their time of occurrence. An FE model is developed to simulate the anticlastic bending test. A code is developed using ANSYS Parametric Design Language to obtain the first ply failure predictions of maximum stress, maximum strain, Tsai-Wu, Tsai-Hill, Hashin, Hoffman and quadric surfaces failure criteria. The experimental and numerical results are then compared. Relative strengths and weaknesses of the failure criteria in estimating failure of laminated composite plates under anticlastic bending are determined.

ÖZET

ÇİFT EKSENLİ EĞİLME YÜKLEMESİ ALTINDAKİ KATMANLI KOMPOZİT PLAKALARIN KIRILMA DAVRANIŞININ İNCELENMESİ

Bu çalışmada anticlastic eğme yüklemesine maruz kalan katmanlı bir kompozit plakanın kırılma davranışı incelenmiştir.Anticlastic eğme, bükme momentinin etkin moment olduğu bir çift eksenli yükleme çeşididir. Bu yükleme koşullarını sağlayacak şekilde özgün bir deney aparatı tasarlanmıştır. Toplam sekiz farklı konfigürasyona ait dörder numune test edilmiştir.Numunenin alt ve üst tarafataki tüm kenarlarına delaminasyon riskini azaltmak ve destek şeritleri çekilmiştir. İlk hasarın oluştuğu yeri tespit edebilmek için akustik emisyon izleme (AEM) cihazı kullanılmıştır.Bu yöntem ile ilk ve ilerleyici hasar mekanizması ve zamanı tespit edilebilmektedir. Çalışmada anticlastic eğme yükünü simule edebilmek için sonlu elemanlar yöntemiyle modelleme yapılmıştır. ANSYS Parametrik Programlama Dili kullanılarak, maksimum gerilme, maksimum genleme, Tsai-Wu, Tsai-Hill, Hoffman, Hashin ve quadric surfaces kırılma kriterlerinin öngörüleri tespit edilmiştir. programı kullanılarak bir analiz kodu geliştirilmiştir. Deneysel ve sayısal sonuçlar karşılaştırıldığında ilgili kırılma kriterlerinin anticlastic eğme yüklemesi altındaki katmanlı kompozit plakanın kırılma davranışının öngörülmesi konusundaki güçlü ve zayıf yanları gösterilmiştir.

TABLE OF CONTENTS

LIST OF FIGURES

LIST OF TABLES

LIST OF SYMBOLS

F	Force
M_{xx}	Moment in x direction
M_{yy}	Moment in y direction
M_{xy}	Twisting moment
X	Strength in fiber direction
X_c	Compression strength in fiber direction
X_t	Tensile strength in fiber direction
Y	Strength in transverse direction
Y_c	Compression strength in transverse direction
Y_t	Tensile strength in fiber direction
$Y\varepsilon_t$	Compression strength in terms of strains in transverse direction
$Y\varepsilon_t$	Tension strength in terms of strains in transverse direction

LIST OF ACROYNMS/ABBREVIATIONS

2D	Two dimensional
3D	Three dimensional
AE	Acoustic emission
AEM	Acoustic emission monitoring
APDL	Ansys Parametric Design Language
CFRP	Carbon-Fiber Reinforced Polymers
FEM	Finite Element Analysis
FFT	Fast fourier transform
HDT	Hit definition time
HLT	Hit lockout time
MPa	Megapascal
kHz	Kilo hertz
mm	Milimeter
PDT	Peak definition time
SOLID185	Layered 3-D Solid Element

1. INTRODUCTION

Composite materials are preferred in the industry mainly due to their high specific strength (strength-to-weight ratio) and specific stiffness (stiffness-to-weight ratio). The stacking sequence of laminates can be tuned to attain better performance for different applications.

Laminated composite plates exhibit much more complex behavior than conventional materials. Interactions between fibers and matrix, existence of different failure modes like delamination, fiber breakage, matrix cracking, buckling of fibers, debonding of fibers from matrix, predominance of a different failure mode over the others under a different loading state or a different layup pose great difficulty.

The most common failure mode in laminated composite plates is matrix cracking [1]. Because matrix is the weakest part of a fiber-reinforced plastic composite, matrix micro cracks start first under loading. In a laminated composite, fibers and matrix are bonded to each other. But, because of the mismatch in the stiffness and thermal properties, they are debonded after a load limit. This phenomenon is called fiber-matrix debonding (Figure 1.1). After debonding, since the shearing force which holds the fiber in its original place is reduced, fibers are more prone to be pulling-out [1]. In most cases, fiber-matrix debonding and fiber pull-out successively occur [1]. An important failure mechanism observed in laminated composites is delamination. Delamination may occur as a result of geometrical discontinuities, mismatch of the material properties, tensile stresses at the edges of the part, or the out-of-plane loads [1]. Safe design of composite parts requires failure models that accurately predict failure of composites with a given layup under a given loading condition

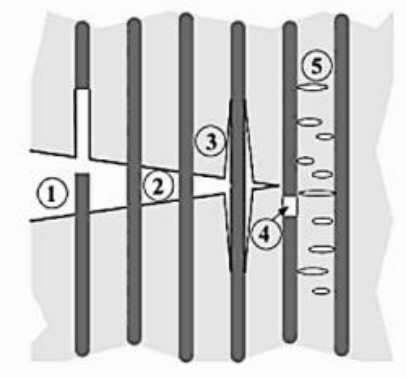

Figure 1.1. The schematic respresentation of (1) fiber pull-out (2) fiber-matrix debonding (4) fiber failure (5) matrix cracking [1].

A number of static failure theories have been introduced for composite materials [2-13] like maximum stress, maximum strain, Tsai-Wu, Tsai-Hill, Hoffman, Hashin and quadric surfaces. In general, failure criteria are based on stress or strain. These failure criteria are either use the stress state developed in the laminate like Tsai-Wu or strain state like maximum strain criterion. . They may be linear like maximum stress or quadratic like Tsai-Wu. Some can predict the failure mode like maximum stress, maximum strain and Hashin; some cannot like Tsai-Wu, Tsai-Hill, and Hoffman.

In industrial applications, designers face the difficulty of safely designing composite parts under complex loading cases. So understanding the failure behavior of the material under different loading conditions gains importance. Failure mechanisms and response of laminated plates are extensively studied and validity of the failure criteria is investigated for in-plane loading conditions [15-19]. On the other hand, not sufficient attention has been given to out-of-plane loading. Many composite structural parts like aircraft wings and wind turbine blades are subjected to a combination of bending and twisting moments or transverse forces. Failure analyses of composites based on failure criteria validated only for in-plane loading cannot be considered to be reliable, if the part is subjected to out-of-plane loads. Hence, reliable design of laminated composite parts requires use of failure theories validated for various loading conditions.

In the literature, there are a number of studies that examined the failure behavior of laminated composite under various out-of-plane loads and investigated the validity of different failure criteria. Hara *et al*. [20] combined experimental and FEA procedures with Weibull statistics and compared the out-of-plane strengths of carbon-fiber-reinforced plastics (CFRP) under direct loading and three-point bending. Feraboli and Kedward [21] investigated the flexural and interlaminar shear strength of the unidirectional and multi-directional CFRP's using four-point bending.

In the literature, usually four-point-bending [21] or three-point-bending [20] tests were conducted to study the out-of-plane failure behavior of composites. In these tests, specimens were predominantly subjected to uniaxial bending, M_{xx} or M_{yy}. In the tests where transverse loads were applied, specimens were predominantly subjected to bi-axial bending (both M_{xx} and M_{yy}) as seen in Figure 1.2a. On the other hand, in anticlastic loading, specimen is predominantly subjected to twisting moment, M_{xy}. This loading state is realized either by applying bending moments in opposite sense (Figure 1.1b) or by applying force couples having the same magnitude but opposite direction to the neighboring corners of a square plate as shown in Figure 1.1c. Farsad *et al*. [22] used anticlastic bending to determine the shear modulus and Poisson's ratio of some polymers and foams. In another research, Farshad [23] investigated the mode III fracture toughness of various materials including CFRP and GFRP by means of anticlastic bending. Podczeck [24] used this method to determine the fracture properties of some pharmaceutical materials. However, anticlastic bending has not been used to investigate the static failure behavior of composite materials.

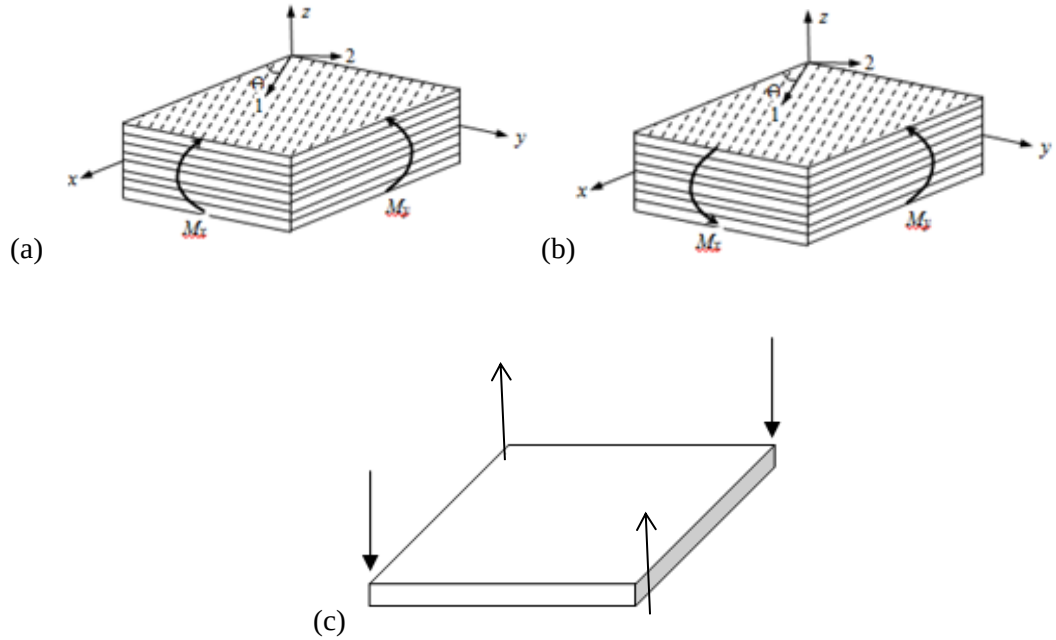

Figure 1.2. (a) Bi-axial bending applied by two bending moments in the same sense, (b) Anticlastic bending applied by two bending moments in opposite sense, (c) Anticlastic bending applied by force couples.

In this study, the strength of continuous fiber-reinforced laminated composite plates with different stacking sequences are investigated under anticlastic bending and validity of selected failure criteria is examined under this loading state. For this purpose, a unique anticlastic bending test apparatus is designed. Laminated plates with 100 mm × 100 mm dimensions and 12-ply thickness are manufactured. The progressive failure behavior of the specimens is monitored and failure modes are detected during testing by means of acoustic emission monitoring (AEM). The test is simulated by developing a finite element model in ANSYS and a code is developed using ANSYS parametric design language (APDL) to employ the selected failure criteria. The experimental results and predictions of the failure criteria are compared and the criteria which yield the most realistic results are determined for each stacking sequence. In this way, the validity of chosen failure criteria is investigated for this type of loading condition and valuable information is provided for the designers as to the reliability of their failure analyses.

2. FAILURE CRITERIA

In order to ensure the safety of composite laminated plates against failure without using a large safety factor, reliable failure theories are needed that will correctly predict whether the plate will fail or not under given loading conditions for a given laminate configuration. Validity of a failure theory may only be shown by comparing its predictions with the experimental data. Recognizing that in-plane and out-of-plane responses of composite laminates are quite different, one may not conclude that a failure theory validated for in-plane loads is also valid under out-of-plane loading conditions. For this reason there is a need to examine the validity of the failure criteria for different types of loads. Only in this way, safety of the design can be ensured during a design process. In real applications, laminates are usually subjected to multi-axial loading, which may be in-plane or out-of-plane.

Researchers studied laminated composites subjected to in-plane multiaxial loads both experimentally and theoretically and examined validity of the failure theories. On the other hand, laminated composite plates under out-of-plane loads were not studied adequately and also the available studies mostly considered plates under uniaxial bending.

In this study, seven widely used failure criteria are selected and used to predict the failure load of the specimens for the chosen stacking sequences under anticlastic loading.

2.1. Tsai-Wu Criterion

Tsai-Wu criterion is an extended version of Von-Misses criterion. According to this criterion [2],the failure will initiate when;

$$F_1\sigma_1 + F_2\sigma_2 + F_6\tau_{12} + F_{11}\sigma_1^2 + F_{22}\sigma_2^2 + F_{66}\tau_{12}^2 + 2F_{12}\sigma_1\sigma_2 + 2F_{16}\sigma_1\tau_{12} + 2F_{26}\sigma_2\tau_{12} > 1 \quad (2.1)$$

After substituting the constants F_1, F_{11}, F_2, F_{22}, F_6, F_{66}, F_{16}, F_{26} and F_{12} , the criteria becomes

$$\left(\frac{1}{X_t}+\frac{1}{X_c}\right)\sigma_1+\left(\frac{1}{Y_t}+\frac{1}{Y_c}\right)\sigma_2-\frac{\sigma_1^2}{X_tX_c}-\frac{\sigma_2^2}{Y_tY_c}+\frac{\sigma_{12}^2}{{S_{12}}^2}-\frac{\sigma_1\sigma_2}{\sqrt{X_tY_tX_cY_c}}\geq 1 \tag{2.2}$$

where '1' and '2' are subscripts signifying the fiber direction and the transverse direction, respectively. 'X,' 'Y,' and 'S_{12}' denote the strengths in 1 and 2 directions and the shear strength in 1-2 plane respectively. 't' and 'c' refers to tension and compression, respectively.

2.2. Maximum Strain Criterion

Failure is decided based on strain components in the principal material coordinates, ε_1, ε_2 and, ε_{12}. According to this criterion, failure occurs, if one of the following conditions is not satisfied:[3];

$$X_{\varepsilon c}<\varepsilon_1<X_{\varepsilon t} \tag{2.3}$$

$$Y_{\varepsilon c}<\varepsilon_2<Y_{\varepsilon t} \tag{2.4}$$

$$|\varepsilon_{12}|<S_\varepsilon \tag{2.5}$$

Principle strains are to be found by using transformation matrix:

$$\begin{bmatrix}\varepsilon_1\\ \varepsilon_2\\ \varepsilon_{12}\end{bmatrix}=[T]\begin{bmatrix}\varepsilon_x\\ \varepsilon_y\\ \varepsilon_{xy}\end{bmatrix} \tag{2.6}$$

2.3. Maximum Stress Criterion

This criterion predicts failure, if the stress components in the principal material direction, σ_1, σ_2, and σ_{12}, do not satisfy one of the following equations [2].

$$X_t < \sigma_1 < X_c \tag{2.7}$$

$$Y_t < \sigma_2 < Y_c \tag{2.8}$$

$$|\tau_{12}| < S_{12} \tag{2.9}$$

2.4. Tsai-Hill Failure Criterion

Hill [4] introduced a stress based, quadratic, failure mode independent criterion which accounts for stress interaction. According to the criterion failure occurs if Equation 2.12 is satisfied:

$$(G+H)\sigma_1^2 + (F+H)\sigma_2^2 + (F+G)\sigma_3^2 - 2H\sigma_1\sigma_2 - 2G\sigma_1\sigma_3 - 2F\sigma_2\sigma_3 + 2L\sigma_{23}^2 + 2M\sigma_{13}^2 + 2N\sigma_{12}^2 \geq 1 \tag{2.12}$$

where F, G, H, L, M and N are characteristic parameters. Considering that the material is transversely isotropic, Equation 2.2 becomes under plane stress condition as follows:

$$\left(\frac{\sigma_1}{X}\right)^2 - \frac{\sigma_1\sigma_2}{X^2} + \left(\frac{\sigma_2}{Y}\right)^2 + \left(\frac{\sigma_{12}}{S}\right)^2 \geq 1 \tag{2.13}$$

where X and Y are either tensile or compression strengths depending on the sign of respective stresses.

2.5. Hoffman Failure Criterion

Hoffman's failure criterion [7] is stress-based and a modified version of Hill's criterion obtained by adding linear terms. According to this criterion, failure occurs if the equation below is satisfied;

$$C_1(\sigma_y - \sigma_z)^2 + C_2(\sigma_x - \sigma_z)^2 + C_3(\sigma_x - \sigma_y)^2 + C_4\sigma_x + C_5\sigma_y + C_6\sigma_z + C_7\sigma_{yz}^2 + C_8\sigma_{xz}^2 + C_9\sigma_{xy}^2 \geq 1 \quad (2.10)$$

where C_1 , C_2, C_3 ,C_4 C_1 , C_5 C_6 , C_7 , C_8 , C_9 are material parameters which are to be found by means of nine basic strength data, three uniaxial tensile strengths, three uniaxial compressive strengths, three shear strengths.

For plane stress conditions, the equation becomes

$$-\frac{\sigma_1^2}{X_tX_c} + \frac{\sigma_1\sigma_2}{X_tX_c} - \frac{\sigma_2^2}{Y_tY_c} + \frac{X_c+X_t}{X_cX_t}\sigma_1 + \frac{Y_c+Y_t}{Y_cY_t}\sigma_2 + \frac{\sigma_{12}^2}{S_{12}^2} \geq 1 \quad (2.11)$$

2.6. Hashin Failure Criterion

Hashin[6] proposed a stress-based failure criterion which determine the failure mode such as fiber failure under tension, fiber failure under compression, matrix failure under tension, and matrix failure under compression.

Fiber failure under tension:

$$\left(\frac{\sigma_1}{X_t}\right)^2 + \left(\frac{\sigma_{12}}{S_{12}}\right)^2 \geq 1 \qquad \text{if } \sigma_1 > 0$$

Fiber failure under compression:

$$\sigma_1 \leq \sigma_c \qquad \text{if} \qquad \sigma_1 < 0$$

Matrix failure under tension:

$$\left(\frac{\sigma_2}{Y_t}\right)^2 + \left(\frac{\sigma_{12}}{S_{12}}\right)^2 = 1 \qquad \text{if } \sigma_2 > 0$$

Matrix failure under compression:

$$\left(\frac{\sigma_2}{2S_{23}}\right)^2 + \left[\left(\frac{Y_c}{2S_{23}}\right)^2 - 1\right]\frac{\sigma_2}{Y_c} + \left(\frac{\sigma_{12}}{S_{12}}\right)^2 = 1 \qquad \text{if } \sigma_2 > 0$$

where S_{23} is the maximum allowable shear stress in the 2-3 plane.

2.7. Quadric Surfaces

Quadric surfaces is a stress based failure criterion. The generalized form of the failure function ,f, is given in Equation 2.14 [8];

$$f= A_{ii}\sigma_i^2 + A_{jj}\sigma_j^2 + A_{ij}\sigma_{ij}^2 + B_{ij}\sigma_i\sigma_j + C_{ij}\sigma_i\sigma_{ij} + D_{ij}\sigma_j\sigma_{ij} + F_i\sigma_i + F_j\sigma_j + F_{ij}\sigma_{ij} \geq 1 \quad (2.14)$$

for i, j=1,2,3, where, A_{ii}, A_{jj}, A_{ij}, B_{ij}, C_{ij}, D_{ij}, F_i, F_j, F_{ij} are characteristic parameters and the repeated index is not summed. Quadric surfaces criterion claims that failure occurs under plane stress condition in a composite plate if Equation 2.15 is satisfied.

$$\frac{a}{X^2}\sigma_1^2 + \frac{a}{Y^2}\sigma_2^2 + \frac{a}{S^2}\sigma_{12}^2 + \frac{b}{XY}\sigma_1\sigma_2 + \frac{b}{XS}\sigma_1\sigma_{12} + \frac{b}{YS}\sigma_2\sigma_{12} + \frac{c}{X}\sigma_1 + \frac{c}{Y}\sigma_2 + \frac{c}{S}\sigma_{12} \geq 1 \quad (2.15)$$

where a= 0,98, b= 0,49 and c=0,002.

3. EXPERIMENTS

3.1. Experimental Set-up

A unique experiment set-up is designed to apply anti-clastic bending to laminated plates. Specimens are placed on two spherical steel supports, which hold the specimen at points on the diagonal close to corners, as shown in Figure 3.1. Support points are 15 mm away from the intersecting edges and $15\sqrt{2}$ mm away from the corners. Rubber bands are placed between the balls and the specimen to reduce stress concentration. Pin supports are fixed to the bottom portion of the set up to ensure the proper alignment of the specimens during testing as shown in the Figure 3.1. The prismatic supports are placed on a sliding base to accommodate different specimen sizes.

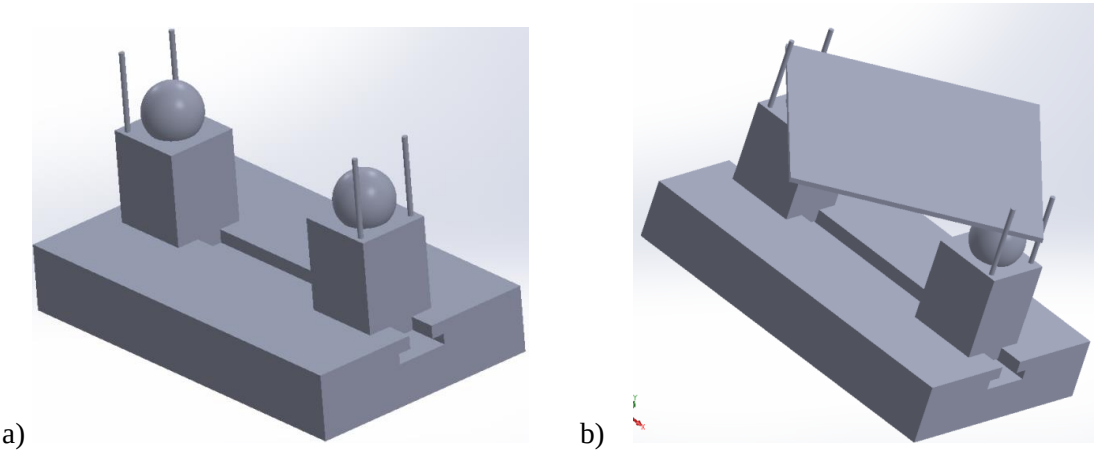

Figure 3.1. a) The bottom portion of the test apparatus b) The bottom portion of the test apparatus with specimen.

3.2. Specimen preparation

In this study, composite plates are manufactured from AS4/8552 unidirectional composite pre-pregs. First, they are cut into the shape of a square with 300 mm-length edges. Then, they are laid up with desired stacking sequence and thickness. In order to observe how successfully the failure criteria predict the failure trend, i.e. the change in the failure load with a change in the orientation angle, θ, unidirectional $[\theta_{12}]$, and symmetric-

balanced, $[(\theta/-\theta)_3]_s$, layup configurations are chosen, which are $[0_{12}]$, $[5_{12}]$, $[15_{12}]$, $[30_{12}]$, $[45_{12}]$ and $[(5/-5)_3]_s$, $[(15/-15)_3]_s$, $[(30/-30)_3]_s$, $[(45/-45)_3]_s$. Note that due to the symmetry in geometry and loading, $[\theta_{12}]$ and $[(90^o-\theta)_{12}]$ configurations or $[(\theta/-\theta)_3]_s$ and $[(90^o-\theta/90^o-\theta)_3]_s$ configurations yield the same result. Additionally, cross-ply configurations, $[(90/0)_3]_s$ and $[90_3/0_3]_s$, are tested. There are minimum four specimens tested for each sequence. Three of them are stripped specimen, the other is non-stripped specimen for comparing the acoustic emission results. The thickness of one ply is 0,184 mm according to the product catalogue. The edges of the specimens are rubbed in order to minimize the notch effect. Unidirectional specimens are cut, stacked and consolidated as 220mm x 220 mm plates and then cut by electric saw so as to obtain four 100 mm x 100 mm square specimens. For multidirectional plates, pre-pregs are cut as 300 mm x 300 mm unidirectional plies and then each stack is cut with the desired orientation angle. All plies of the laminates are stacked manually. The orientations of the plies with respect to loading line is shown in the Figure 3.2 schematically. ‘θ’ represents the orientation angle and center of the circles represents loading points of the laminated composite.

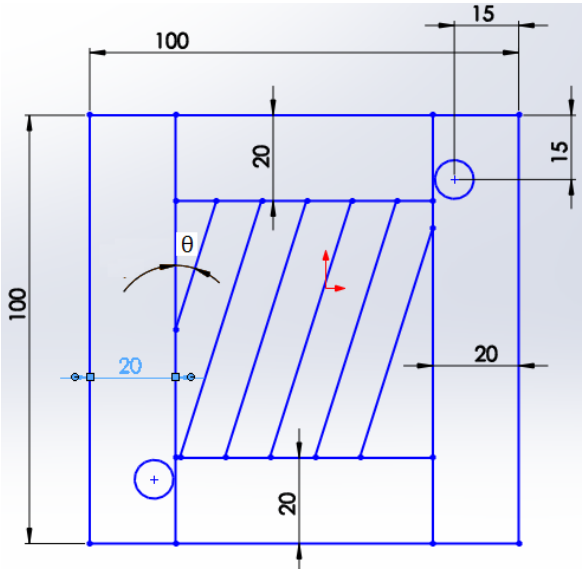

Figure 3.2. Schematic of orientation angle and loading points of the laminate.

3.3. Manufacturing Process

All composite plates are consolidated and cured in autoclave. In composite laminate manufacturing, autoclave curing has traditionally been used to achieve high quality

composites with the desired resin-to-fiber ratio and low void content. Autoclave is a pressure chamber which applies vacuum to the laminate before curing starts, then pressurized during heated cure cycle according to the given recipe [35].

The following procedure is used to manufacture the composite plate in the autoclave;

(i) Stacked composite plates are laid on the table of the autoclave. The table is covered with Teflon so as to prevent the plates sticking on the table as well as to have a smooth surface. Specimens are covered with Teflon and steel plates with the same size are put on the plates to obtain a smooth top surface as well. (Figure 3.3)

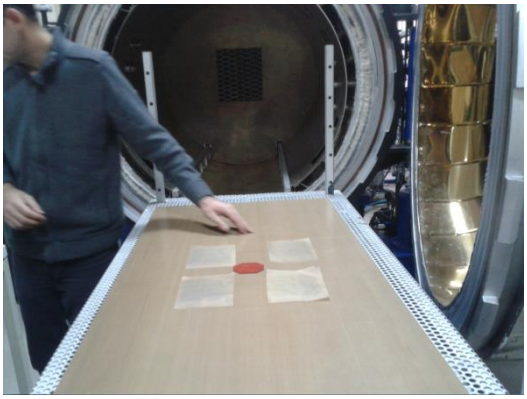

Figure 3. 3. Placement of the stacked plates the specimens on the table with a Teflon cover.

(ii) The bottom components of the vacuum apparatus are placed to the middle of the specimens and breather is laid on the specimens as seen in Figure 3.4. The Breather is used to ensure a homogenized vacuum pressure.

Figure 3. 4. Placing the breather, bottom portion of the vacuum apparatus and sealing strip.

(iii) A sealing strip is stuck around the specimens and the vacuum bag (Figure 3.5). After providing proper sealing, the vacuum apparatus is set to the desired vacuum pressure which is 1.0 bar (Figure 3.6). Vacuum pressure is 1 bar according to the curing cycle recipe of the material.

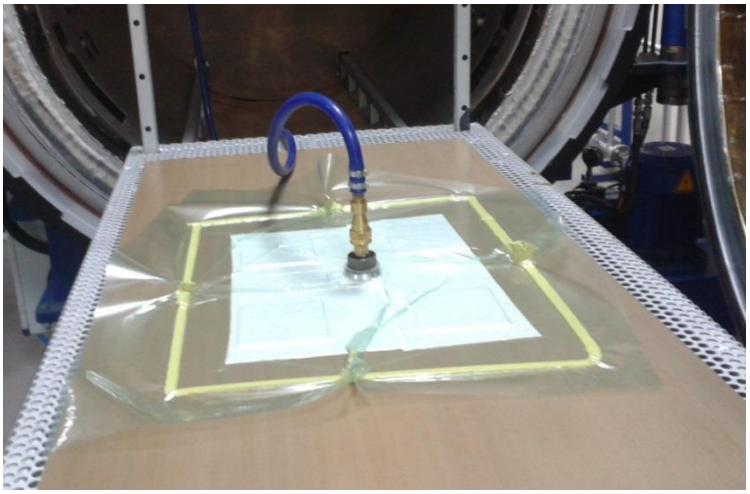

Figure 3. 5. Specimens, ready for the curing cycle.

(iv) The cure cycle recipe shown in Figure 3.6 is input to the controller of the autoclave machine.

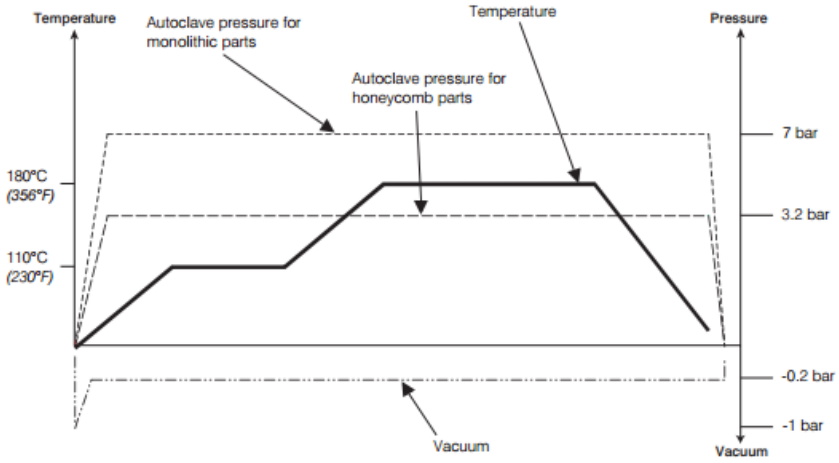

Figure 3. 6. The cure cycle [31].

The curing cycle involves heating the laminates to 120^{o} at the speed of 1-3^{o}C /min and holding at this temperature for 60 minutes, then increasing the temperature with the same speed to 180^{o}C and holding at this temperature for 120 minutes, then cooling down to the room temperature at the speed of 2-5^{o} /min. The external pressure is kept at 7.0 bars, while vacuum pressure is 1.0 bar during all cure cycle.

3.4. Acoustic Emission Monitoring (AEM)

AEM is a non-destructive testing method which is capable of discriminating the different failure modes by detecting different acoustic signals produced by specimens. AE monitoring device mainly provides the AE feature data of all recorded acoustic signals. The basic AE features are rise time, duration, energy, absolute energy, signal strength and amplitude. An important feature of the AEM is real-time monitoring. In addition, this method enables one to locate the source of the failure if three or more transducers are employed.

Usually, it is difficult to experimentally determine the first ply failure load of composite materials unless the first and final loads are the same. This is because the initiation of damage usually does not cause significant change in macro behavior of the specimens. AEM provides a powerful tool for predicting the first-ply failure load, progression of load, and even the failure mode. Basic failure mechanisms in laminated

composite materials are matrix cracking, fiber-matrix debonding, delamination, fiber buckling and fiber breakage. Each failure mode generates its characteristic AE signal.

Some different AE evaluation approaches have been proposed to discriminate the failure modes of materials.

3.4.1. Parameter Based Approach

This approach considers AE features to classify the data ranges corresponding to different failure modes. Gong *et al*. [25] proposed an amplitude range for different types of failures of GFRP composites. However, since AE features are highly dependent on the Piezoelectric transducers (Sensors), extracting a global result is not possible in many cases. So Nimdum and Renard [26] used AE features with some other parameters like waveform and FFT diagram and proposed a multivariable method.

3.4.2. Fast Fourier Transform (FFT) Technique

Frequency content of AE hit data provides a powerful tool for understanding the failure mode of the materials. This method is based on classifying the frequency ranges according to the corresponding failure mechanism. De Groot *et al*. [27] classified the frequency content of carbon/epoxy composite materials into four types: Matrix cracking (90-180 kHz), debonding of fiber/matrix (240-310 kHz), fiber pull-out (180-240 kHz) and fiber breakage (>300 kHz). Giordano *et al.* [28] studied the fiber breakage failure mode using a single-fiber specimen and evaluated the frequency content of the AE signals. The signal data of a hit and the frequency content of the corresponding data are given in Figure 3.7a and 3.7b.

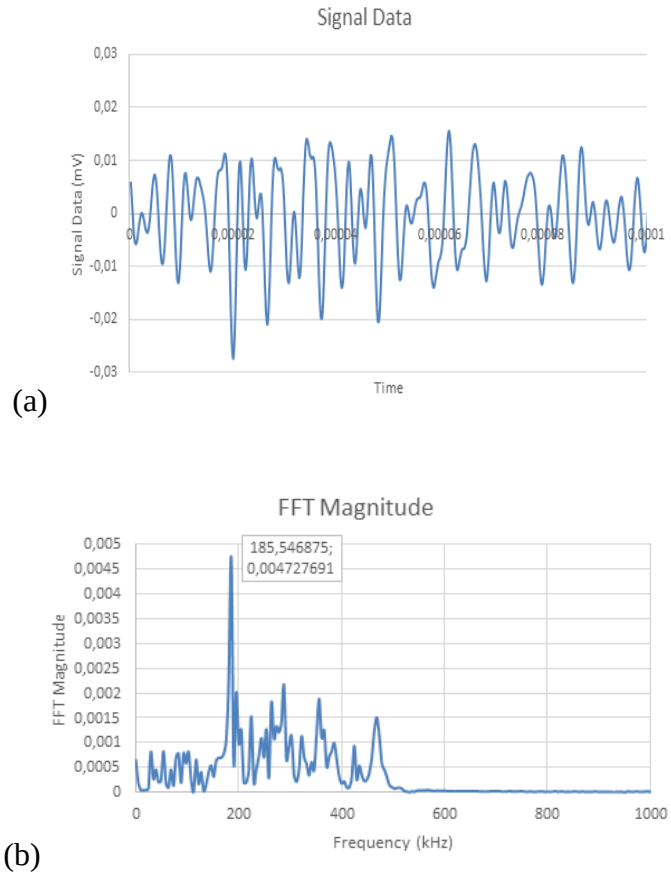

Figure 3. 7. (a) A Signal data of a hit (b) corresponding frequency content.

Beside the failure mode prediction, first-ply failure prediction can be achieved by AEM monitoring. Kam and Lai [29] presented a method to study the first-ply failure strength of laminated composites under different loading conditions. They examined the released energy vs. load diagram and picked the first outstanding peak point of energy (Figure 3.8). When they compared this points' related load value and the results of theoretical first ply failure study, they found a good agreement in any loading condition. Kam and Liu [30] applied this method to a pressure vessel made up with laminated composite and compared this experimental procedure results with the results

In this study, the procedure proposed by Kam and Lai is used [29]. But because extra reinforcing strips are glued to the specimens, the noises coming from the interfaces of specimen and strips are needed to be eliminated to make a correct peak picking. The procedure for first-ply failure prediction and noise elimination is reported in Experimental Procedure section.

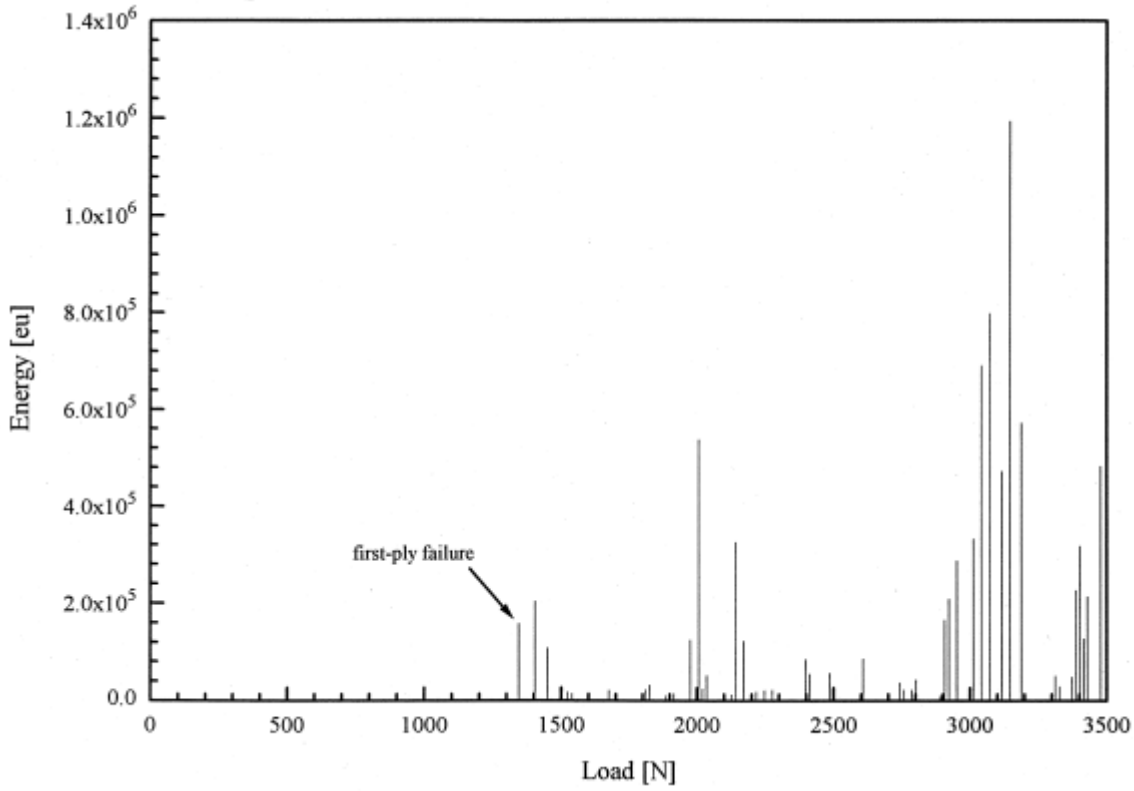

Figure 3. 8. First outstanding peak point of energy corresponding to first-ply failure for laminated composite pressure vessel [29].

3.5. Experimental Procedure

3.5.1. Tension Tests

Because the matrix properties govern the strength and stiffness of the composites in the transverse direction, which in turn determine the first-ply failure strength of multi-directional laminates, transverse strength deserves a special attention. For this reason, instead of using the catalogue value, transverse strength of the composite material was determined through tension tests. of obtaining the realistic value of transverse strength, preliminary tension tests are conducted. Two 12-ply tension test specimens are prepared according to ASTM D3039 standards [36]. Four tabs are bonded to the ends of each specimen as shown in Figure 3.9 in order to ensure that the grips do not damage the specimens and to prevent premature failure. The tabs are 25 mm in width and 50 mm in length. The WELD® glue is used for bonding. The tension tests are conducted on Zwick

Roell tension test machine. Loading capacity of the machine is 10 kN (Figure 3.9). Upper load cell is given 2 mm/min speed upwards. As seen in the Figure 3.10, two AEM transducers are attached to the specimens with grippers. Square rubber bands are put between transducers and grippers and specimens. Extensometer is employed for measuring the displacement of the strain of the specimens.

Tests show that the transverse strength (Table 3.1) is lower than the value given as 63,9 MPa in the manufacturer's catalogue [31].

Table 3.1. Specimen dimensions.

Specimen #	Gage length	width	thickness	Transverse strength
1	150	25.6	2.28	52.5
2	150	25.45	2.25	59.6

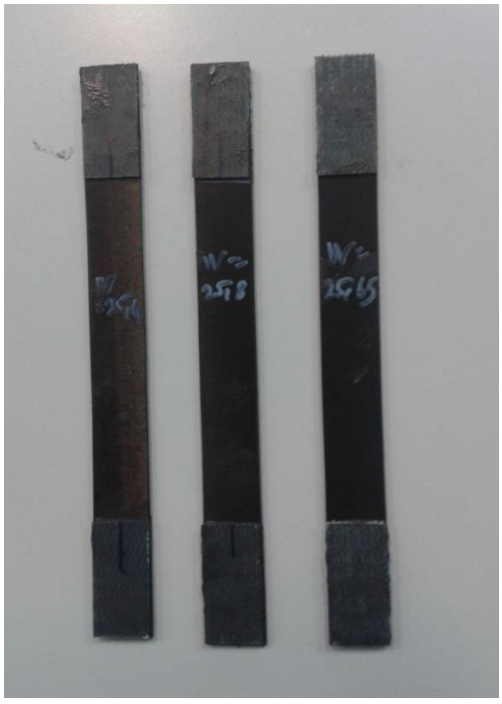

Figure 3. 9. 90^0 tension specimens with tabs.

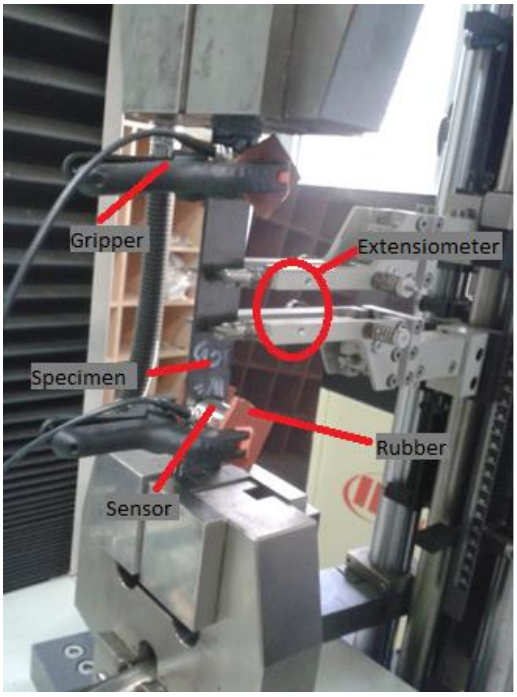

Figure 3. 10. Tension test set up.

3.5.2. Anti-Clastic Bending Tests

After determining the transverse strength of the specimens via tensile tests, anticlastic bending tests are conducted on totally 36 specimens with nine different laminate configurations; that means 4 specimens for each different configuration. Anti-clastic tests are performed in MTS servo-hydraulic test machine using the anticlastic bending fixture. The loading capacity of the machine is 100 kN. Tests are performed as displacement controlled. Bottom load cell is given 1.8 mm/min upward speed. The bottom and top portions of the fixture are attached to the testing machine via connectors. For the sake of reducing the stress concentrations at the points of loads, square rubber bands are placed between the steel balls and the specimen (Figure 3.11).

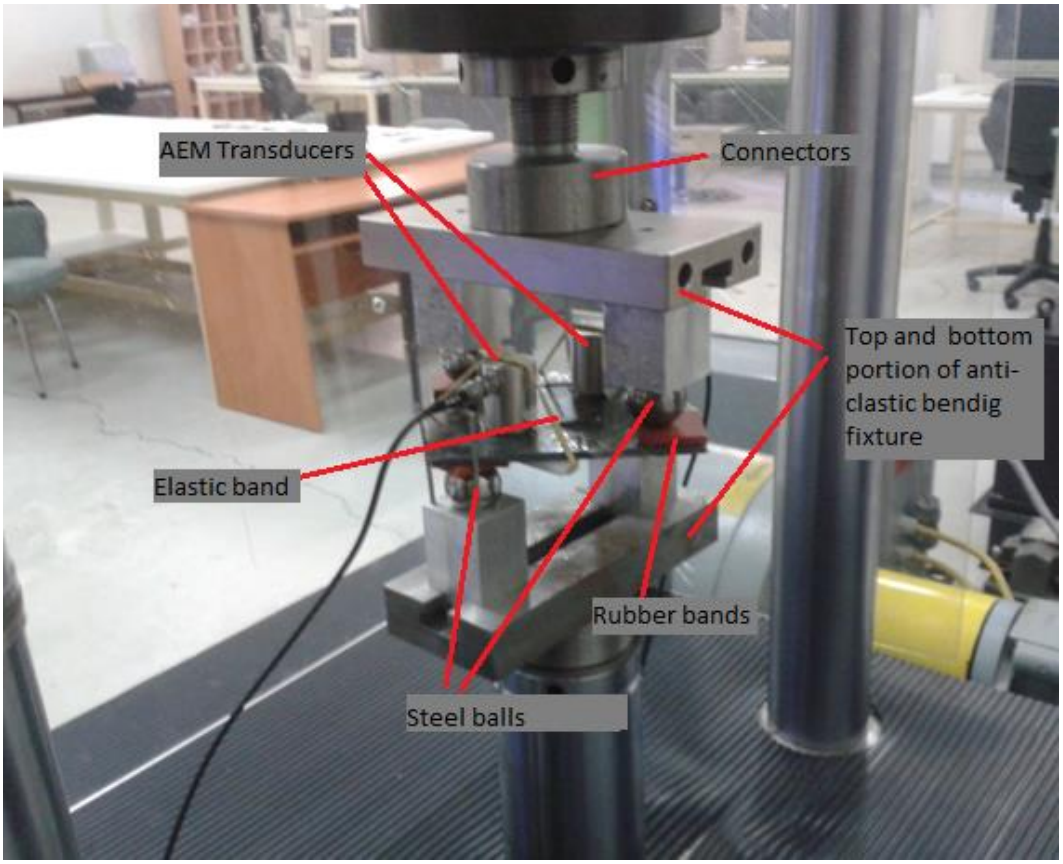

Figure 3. 11. The test apparatus.

3.4.3. Acoustic Emission Monitoring

While performing anti-clastic bending tests, acoustic emission system is run concurrently. In order to collect as much signal as possible, ultrasonic gel is used as couplant. After cleaning the specimen surface, the gel is applied to the transducer surfaces. The transducers are placed symmetrically on the specimen. In order to prevent sliding of the transducers during testing, which may produce noise signals, they are fixed to the pre-determined locations by means of elastic bands and tapes.

The data collected by the acoustic emission device and the test equipment are synchronized after the test by taking the time at the end of the test as the reference time. Since the acoustic emission system starts before the bending test and stops at the same time, the difference between the total times of AE test and the bending test is subtracted from AE test total time. As a result, the two data are synchronized.

All signals coming from the piezoelectric transducers are recorded as hit data. Acoustic emission system produces signals characterized by seven AE features; Amplitude, rise time, counts, duration, energy, absolute energy, signal strength. Amplitude is the greatest measured voltage in the waveform and the unit is dB, rise time is the time interval between the first crossing of the threshold and the signal peak, duration is the time interval between the first and the last threshold crossing, count is the number of pulses emitted by the signal and having higher voltage than threshold value [39], Energy is the area under time versus amplitude curve [40], Signal Strength is signal strength defined as the integral of the rectified voltage signal over the duration of the AE waveform packet [41]. In addition to these features, an important feature is the frequency content. The frequency of a signal can provide important information about failure mode of the material. Because there are a lot of AE hits per test, more than 5000 hits for some tests, a macro code is written in Visual Basic Language embedded in MS Excel.

Defining a proper signal is vital for correct interpretation of the results. There are three timing parameters are to be selected with special attention; Peak definition time (PDT), Hit definition time (HDT) and Hit lockout time (HLT). PDT is the allowable time for determination of peak amplitude of the peak. HDT is the allowable time for the next threshold crossing of the signal, HLT is the duration to start defining a new hit. Timing parameters used in this study are selected in accordance with the recommended values of MISTRAS group [38] as seen in Table 3.2. Detailed information about timing parameters is provided in Appendix A.

Table 3.2. Timing parameters used in this thesis.

PDT	**HDT**	**HLT**
50	100	300

3.4.4. Determination of the First Ply Failure Load

A ‘ Right-hit-determination procedure should be applied to the results of AE test. Because, the bonded reinforcing strips may crack during the test and they may even fully

debond from the specimen surface as seen in Figure 3.12. All these noises are recorded by AEM device and they need to be identified and eliminated in order to distinguish the hit data related to failure of the specimen.

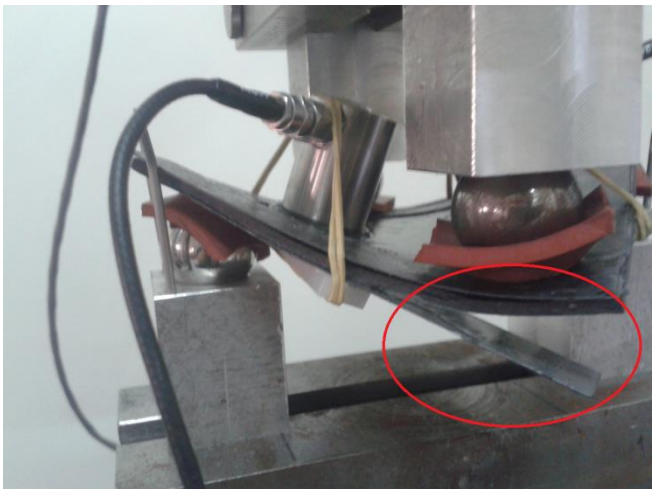

Figure 3. 12. A reinforcing strip debonded from the surface of the specimen.

For the purpose of interpreting the failure modes, frequency ranges for different failure modes introduced by Gutkin *et al*. [42] is used.

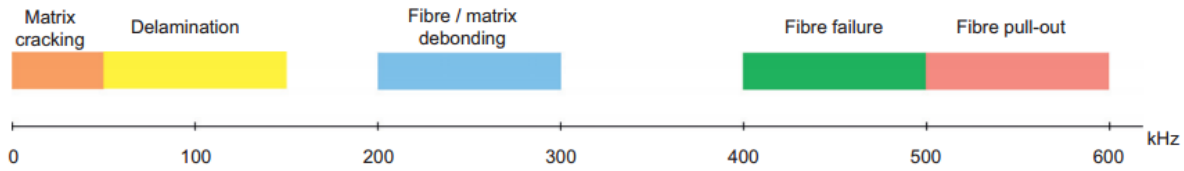

Figure 3.13. Classification of failure modes according to their peak frequencies [42].

In order to discriminate the sounds coming from the specimen and the ones coming from the bonding surface of the reinforcing strips, the frequency contents of the hits are examined because no distinguishing value range in AE features for bonding surface debonding can be obtained. For this purpose, the following procedure is used:

(i) An identically configured non-stripped specimen is also tested for all configurations (Figure 3.14a and 3.14b).

(a)  (b) 

Figure 3.14.(a) Non-Stripped specimen (b) Stripped specimen.

(ii) Stripped and non-stripped test results of unidirectional cases are compared. Since, unidirectional plates are assumed to fail with brittle manner, hits with peak energy value before the ultimate failure load can be assumed to be emitted by reinforcing strip- specimen bonding surface. Figure 3.15 and Figure 3.16 shows this distinguishing characteristic of stripped and non-stripped specimens.

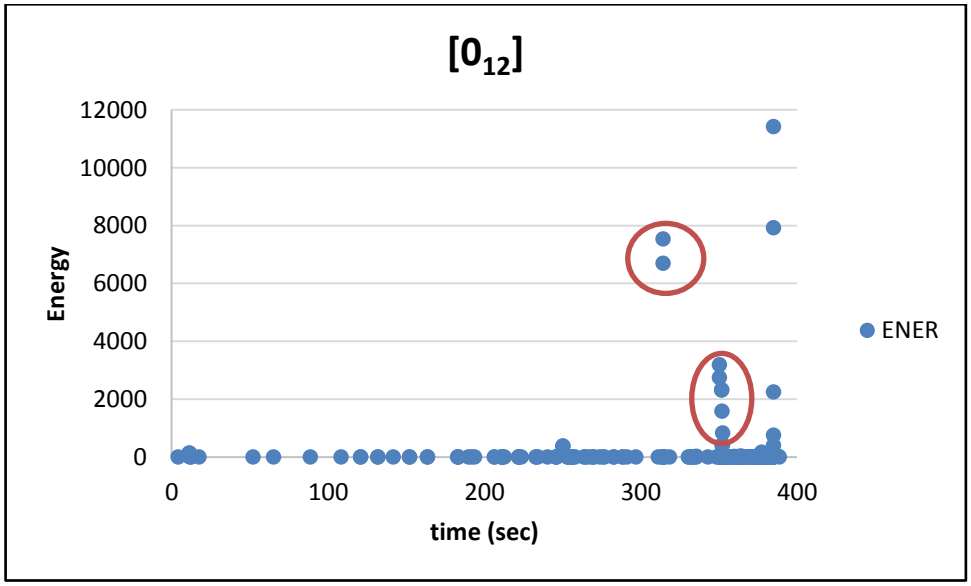

Figure 3. 15. Energy time graph of $[0]_{12}$ configuration specimen showing the signals emitted by bonding surface of strips and specimen.

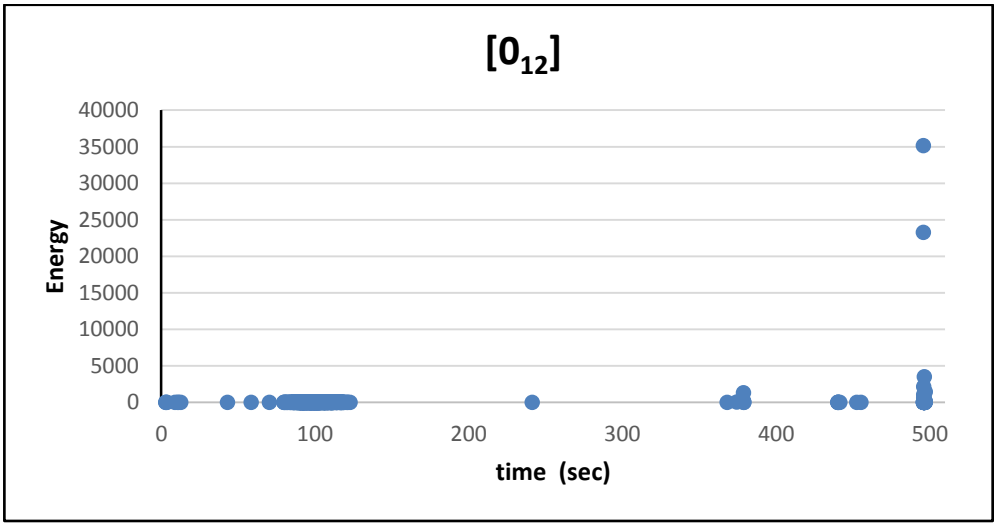

Figure 3. 16. AE result of non-stripped $[0]_{12}$ laminated specimen.

Collecting these distinguished hit data, the frequency range of the emissions of strip-specimen bonding surface is found to be between 110-170 kHz.

(iii) First non-stripped specimen results are checked and the first hit having a peak energy value is determined. The frequency of this hit is the reference frequency value for picking the right hit from stripped specimens. (Figure 3.17)

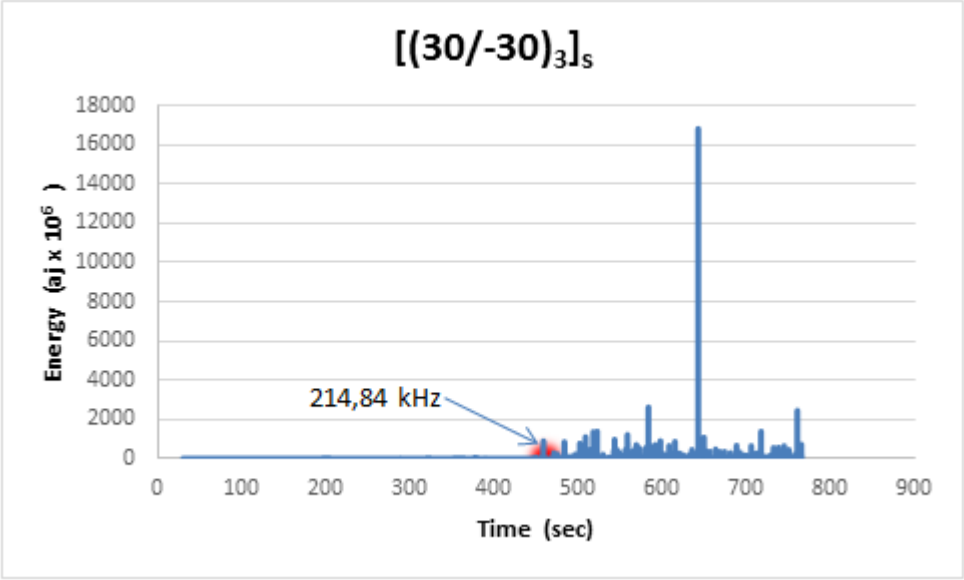

Figure 3. 17. The first peak captured from the $[(30/-30)_3]$s non-stripped specimen.

(iv) The frequencies of the signals recorded after the first energy peak are checked with the time order. The first peak within the same frequency range with the one detected for non-stripped specimen of the same configuration is the peak which starts the first-ply failure. As seen in Figure 3.18, the first peak is caught at the beginning stage of which the energy values begin to peak. It should be noted that the frequency range of 110- 170 kHz may refer either a failure mode or a noise signal emitted by bonding surface. So, if the reference frequency, that is the one found from non-stripped specimen, is determined between 110 and 170 kHz, then an extra procedure may be necessary to distinguish the signals which refer the failure and the noise signals.

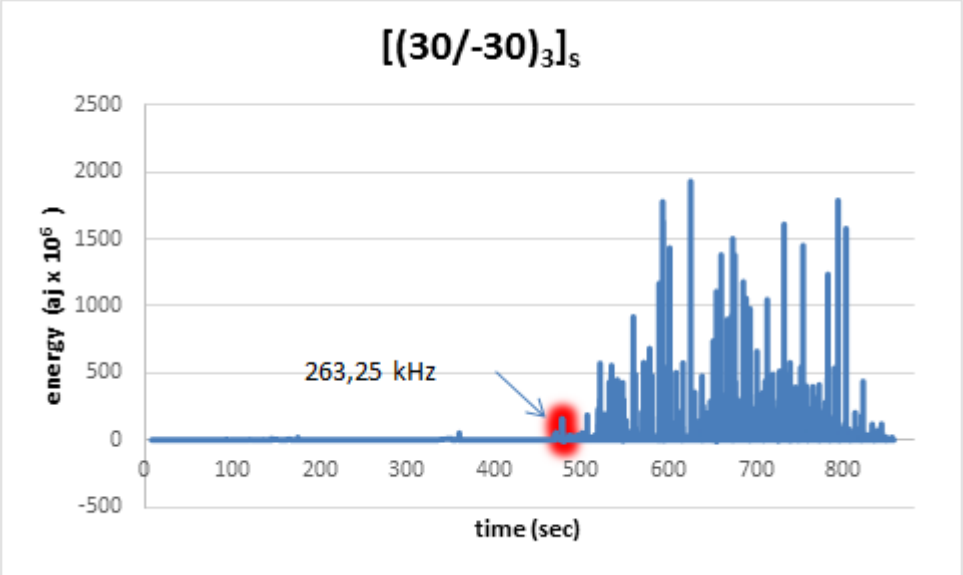

Figure 3. 18. Time-Energy Graph of $[(30/-30)_3]_s$ configuration.

(v) The load value of the picked hit is determined from the Time vs. load graph obtained from the test machine according to the synchronized time data.

4. FINITE ELEMENTS ANALYSES (FEA)

A finite element model is developed to simulate the anticlastic bending test and find the stress and strain states within the specimen using commercial FEA analysis program ANSYS. A code is developed in ANSYS Parametric Design Language (APDL) to apply the failure criteria and predict the first-ply-failure load under the loading conditions of the test.

SOLID185, a layered 3-D structural solid element defined by eight nodes, is used to mesh the structural volume (Figure 4.1). The element has three degrees of freedom at each node, translation in x, y, and z directions [33]. The code is written into a text file and read by Ansys in batch mode.

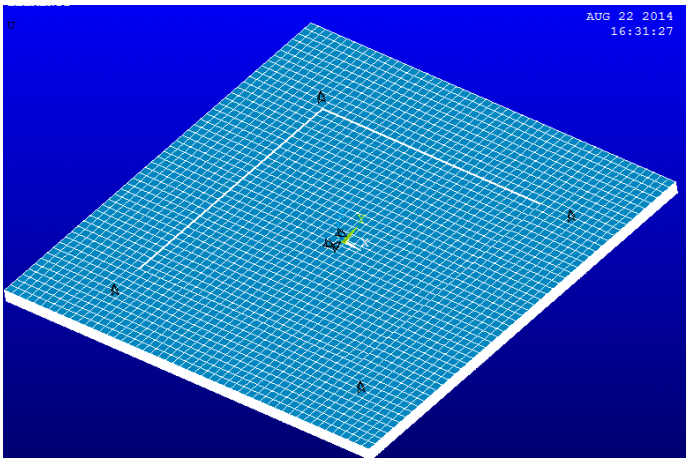

Figure 4.1. The meshed structure of the specimen.

The code is written into a text file and read by Ansys in batch mode. Material properties, except transverse strength, are taken from the technical documents of the material. Transverse strength of the material is determined according to results of conducted tensile tests with 90^0 lay-up tensile test specimens.

Because the tests are conducted under displacement control, displacement boundary conditions are defined in the FE model. In order to prevent rigid body motion in other degrees of freedom, three nodes are selected close to the middle of the specimen and they are held in the x and y directions (Figure 4.1). Displacement values are given to other two diagonal nodes so that the maximum failure index equals to 1.0.

In order to find the applied displacement that causes the maximum failure index to take the value of unity, the secant algorithm is employed. This is an iterative procedure processed within the code starting from two different values for the applied displacement to find the next iteration value until convergence is achieved. The algorithm is given by the following equation:

$$x_n = x_{n-1} - f(x_{n-1}) \frac{x_{n-1} - x_{n-2}}{f(x_{n-1}) - f(x_{n-2})} \quad (1)$$

where, for the present problem, x is the applied displacement in the negative z-direction and f is the corresponding maximum failure index minus 1.0. When the difference between x_n and x_{n-1} becomes very small, the maximum failure index becomes equal to 1.0; that means first-ply failure occurs when the applied displacement has the value of x_n. Then, the corresponding stress and strain states, the deflection, the reaction forces, i.e. the failure load, are extracted from the FE results.

Maximum stress, maximum strain, Tsai-Wu, Tsai-Hill, Hoffman, Hashin and quadric surfaces failure criteria are used to predict the failure load and the corresponding deflection. Among these criteria, the first three criteria are ready to use in Ansys software, but the last three are implemented by the code.

Laminated CFRP specimens are considered as a whole part with the edge strips. Because concentrated forces and sharp edges in the FE model cause stress concentrations more severe than the actual case; these regions are not considered in the failure analysis. There is no trend change observed for 3^o and 1^o of increments of angles as seen in the figure 4.2. Therefore, laminate configurations $[\theta_{12}]$ and $[(\theta/-\theta)_3]_s$ are considered for values of θ from 0° to 45° with 3° of increments. Because of the symmetry in geometry and loading, $[\theta_{12}]$ and $[(90^o-\theta)_{12}]$ configurations or $[(\theta/-\theta)_3]_s$ and $[(90^o-\theta/90^o-\theta)_3]_s$

configurations produce the same result. Some selected multidirectional configurations, $[(90/0)_3]_s$ and $[90_3/0_3]_s$ are also analyzed. The load is applied as point displacement in the negative z-direction to two diagonally symmetric nodes, which are consistent with the real spherical contact. The motion of other two diagonally symmetric nodes is prevented in the z-direction to make them act as support points. The load application points and support points are located 15 mm away from the neighboring edges and $15\sqrt{2}$ mm away from the corners as shown in Figure 4.4.

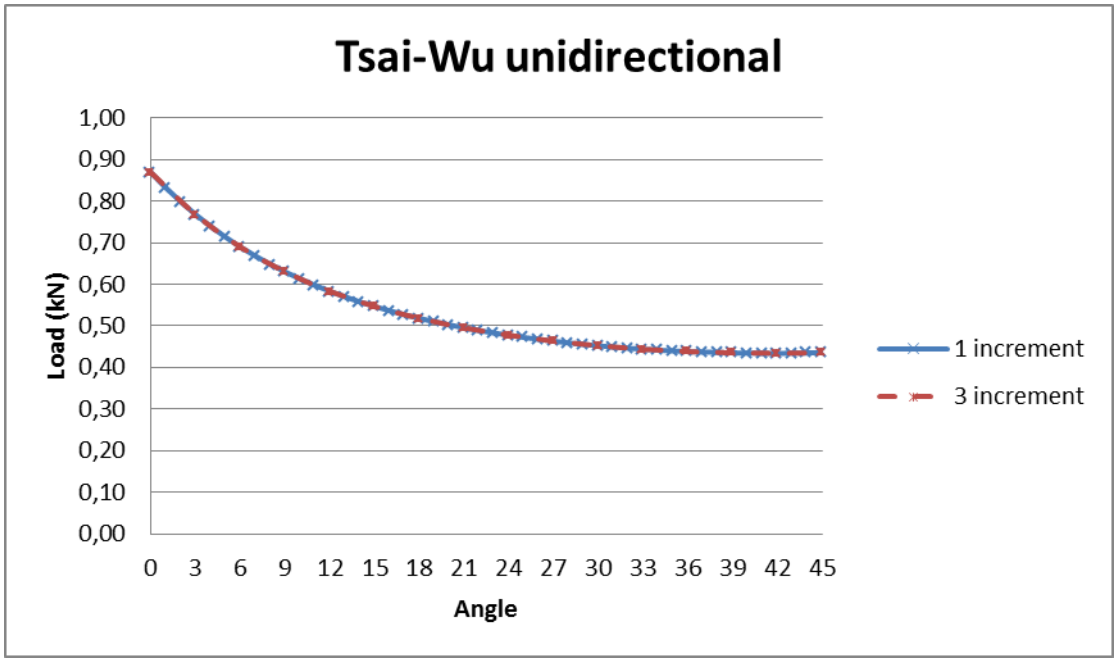

Figure 4.2. Force-angle graph for the Tsai-wu failure criterion for 1^o increment and 3^o of increments.

Convergence analyses are performed to determine the optimum mesh size. Three different element sizes, 1 mm, 2 mm, and 4 mm, are tried, and the differences in the results indicate that that the suitable mesh size is 2 mm. (Figure 4.3).

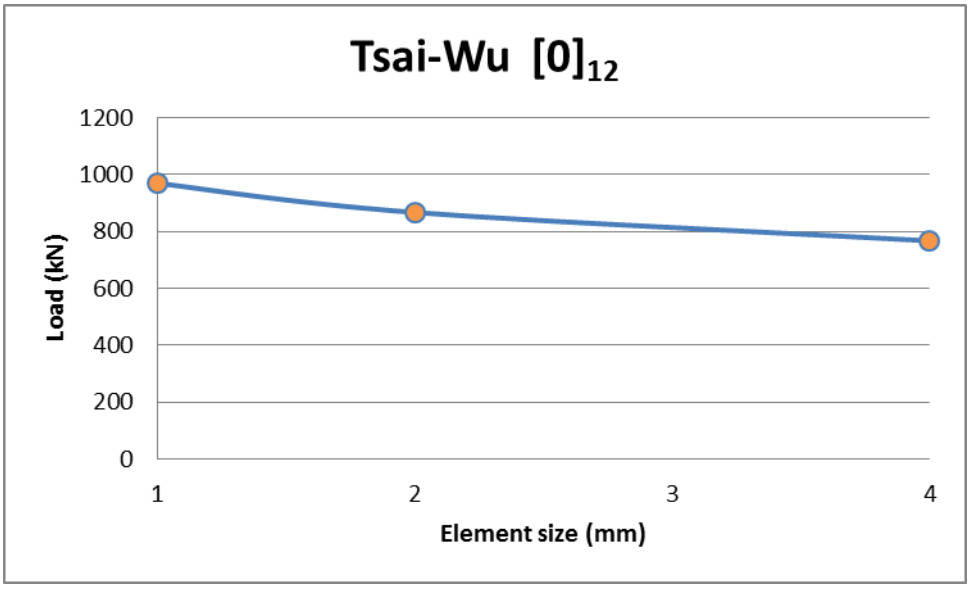

Figure 4.3. Convergence analysis results for Tsai-Wu failure criterion.

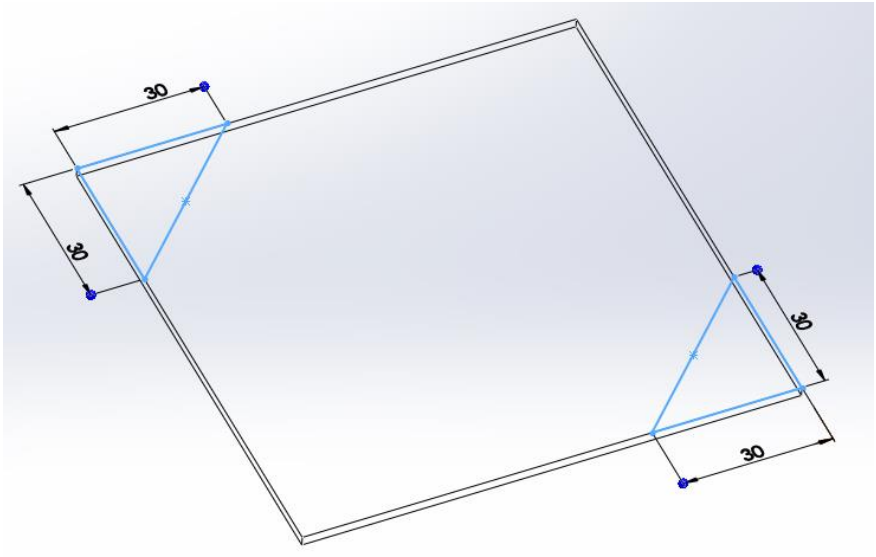

Figure 4.4. Representative loading points on the specimen.

5. RESULTS AND DISCUSSION

Material properties, except transverse strength, are taken from the technical documents of the material [31] and the statistical report [32]. Tables 5.1 and 5.2 [34] show the mechanical properties of AS4/8552 prepreg. The transverse strength of the material is determined by conducting tensile tests on specimens with 90^0 layup.

Table 5.1. Mechanical properties of AS4/8552.

		MEAN VALUE	STANDART DEVIATION	MAX.	MIN.	Average	Error (%)
E_{1t}	STATISTICAL REPORT	131.6 GPa	4 GPa	142.7 GPa	126 GPa	131.69 GPa	2.55
	CATALOGUE	135.14 GPa	-	-	-		
E_{1c}	STATISTICAL REPORT	116 GPa	2.9 GPa	119GPa	105.4 GPa		
	CATALOGUE	128.24 GPa	-	-	-		
E_{2t}	STATISTICAL REPORT	9.24 GPa	0.21 GPa	9.58 GPa	8.89GPa	9.72 GPa	1.42
	CATALOGUE	9.58 GPa	-	-	-		
E_{2c}	STATISTICAL REPORT	9.86 GPa	0.276 GPa	10.34 GPa	9.45 GPa		
	CATALOGUE	-	-	-	-		
v_{12t}	STATISTICAL REPORT	0.302	-	-	-	0.319	4.8
	CATALOGUE	-	-	-	-		
v_{12c}	STATISTICAL REPORT	0.335	-	-	-		
	CATALOGUE	-	-	-	-		
v_{21c}	STATISTICAL REPORT	0.029	-	-	-		
	CATALOGUE	-	-	-	-		
α_1	STATISTICAL REPORT	-	-	-	-		
	CATALOGUE	0.1265×10^{-6}	-	-	-		
α_2	STATISTICAL REPORT	-	-	-	-		
	CATALOGUE	37.12×10^{-6}	-	-	-		

Table 5.2. Strength properties of AS4/8552.

		MEAN VALUE	STANDART DEVIATION	MAX.	MIN
Xt	STATISTICAL REPORT	1928 MPa	87 MPa	2116 MPa	1758 MPa
	CATALOGUE	2137.38 MPa	-	-	-
Xc	STATISTICAL REPORT	1484 MPa	59 MPa	1671 MPa	1408 MPa
	CATALOGUE	1530.64 MPa	-	-	-
Yt	STATISTICAL REPORT	63.9 MPa	6.1 MPa	70.74 MPa	50.3 MPa
	CATALOGUE	80.67 MPa	-	-	-
Yc	STATISTICAL REPORT	267.9 MPa	6.27 MPa	280 MPa	256.6 MPa
	CATALOGUE	-	-	-	-
X_{et}	STATISTICAL REPORT	-	-	-	-
	CATALOGUE	0.0155	-	-	-
X_{ec}	STATISTICAL REPORT	-	-	-	-
	CATALOGUE	-0.012	-	-	-
Y_{et}	STATISTICAL REPORT	-	-	-	-
	CATALOGUE	0.00833	-	-	-
Y_{ec}	STATISTICAL REPORT	-	-	-	-
	CATALOGUE	-0.028	-	-	-
S_{12}	STATISTICAL REPORT	-	-	-	-
	CATALOGUE	0.019	-	-	-
S_{23}	STATISTICAL REPORT	-	-	-	-
	CATALOGUE	0.031	-	-	-

5.1. Experimental Results

Load & energy vs. displacement and frequency & energy vs. displacement graphs of one specimen for each configuration are given in Figures 5.1 to 5.22. The hit signal caused the first-ply failure and the corresponding frequency are indicated on the related energy graph.

As can be noticed in some graphs like $[0_{12}]$, $[5_{12}]$, and $[30_{12}]$, some energy peaks exist before the detected peak which is related to failure. There are three reasons that those peaks are not considered as failure-related peaks. First, they may not correspond to the frequency range under interest; for example in $[0_{12}]$ configuration (Figure 5.1), the peak that occurs at 8.3-mm deflection has 24 kHz frequency, which may indicate minor matrix cracking. Second, they may not initiate a peak-intensive period as in $[45_{12}]$ configuration (Figure 5.9). Third, they may be in the frequency range associated with the strip-specimen surface debonding as in $[30_{12}]$ configuration (Figure 5.7). The breaking points in load-displacement curves, which indicate sudden drops in stiffness, especially encountered in symmetric-balanced laminates are not strictly associated with failure. In some configurations like $[(5/-5)_3]_s$ (Figure 5.11), the second breaking point seems to perfectly overlap the detected failure point. But for some other configurations like $[(15/-15)_3]_s$ and $[(5/-5)_3]_s$, this is not the case. They do not correspond to significant energy peaks detected by the AE equipment. These breaking points may result from slipping between the specimen and the tool or strip-specimen debonding. In some cases, first-ply failure is detected at levels where there is no discontinuity or a changing pattern in the load-deflection curve like in $[(15/-15)_3]_s$, $[(30/-30)_3]_s$, and $[(45/-45)_3]_s$ configurations. In some cases like unidirectional laminates, after the first-ply failure, load carrying capacity significantly degrades, while in some other cases like $[(15/-15)_3]_s$ and $[(45/-45)_3]_s$ ultimate strength is significantly higher that the first-ply failure load level.

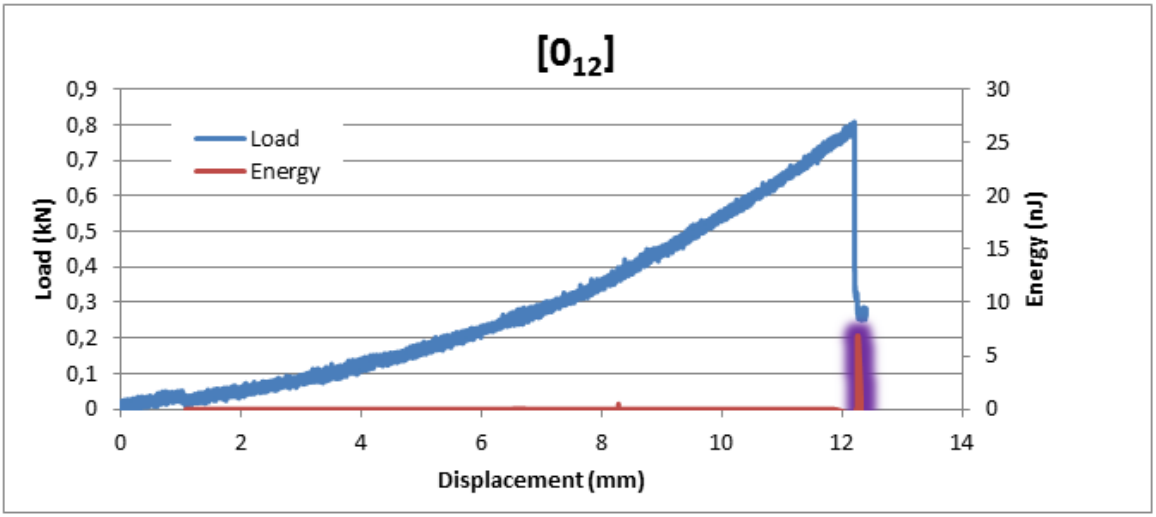

Figure 5.1. Load & energy vs. displacement graph of $[0_{12}]$ configuration laminate.

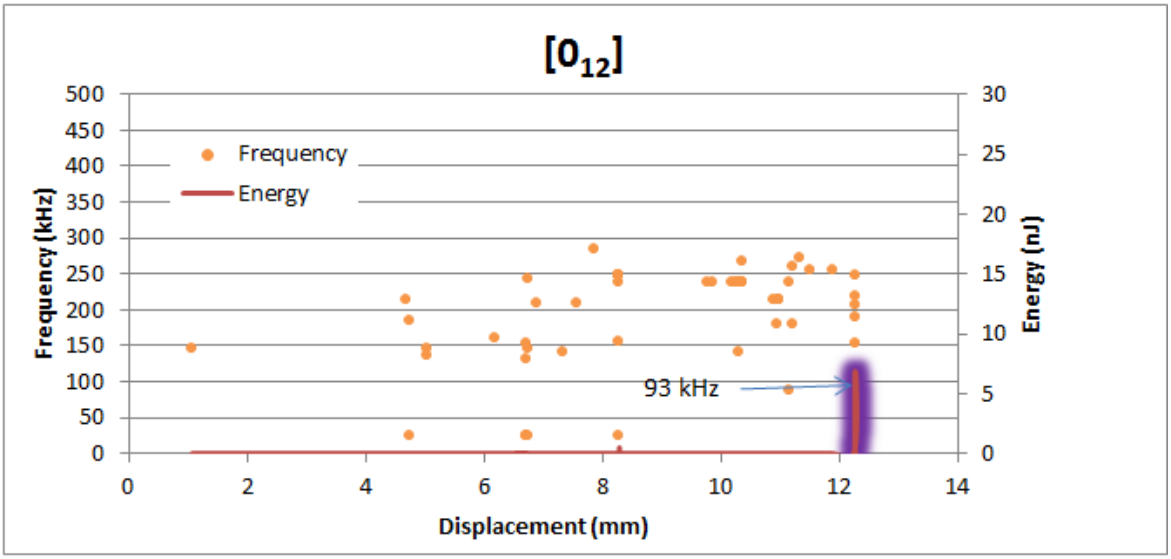

Figure 5.2. Frequency & energy vs. displacement graph of $[0_{12}]$ configuration laminate.

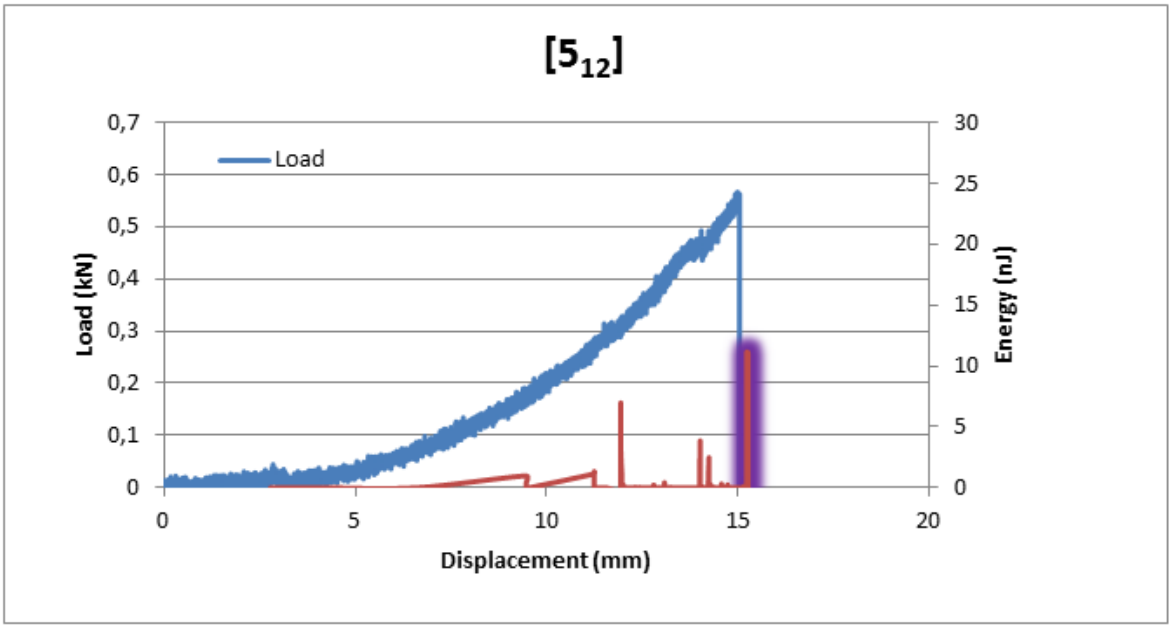

Figure 5.3. Load & energy vs. displacement graph of [5_{12}] configuration laminate.

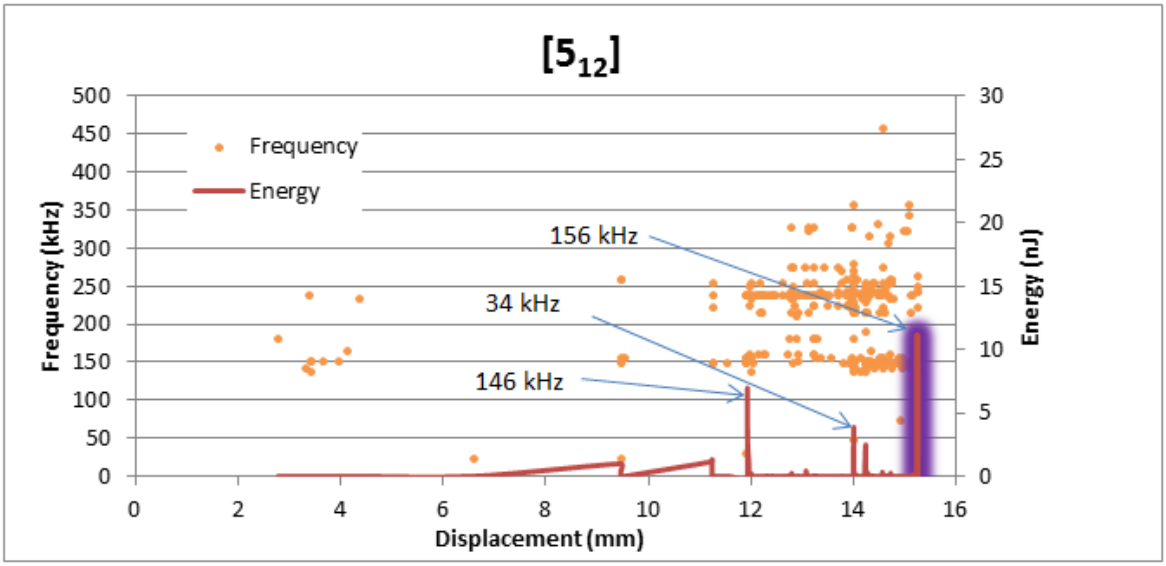

Figure 5.4. Frequency & energy vs. displacement graph of [5_{12}] configuration laminate.

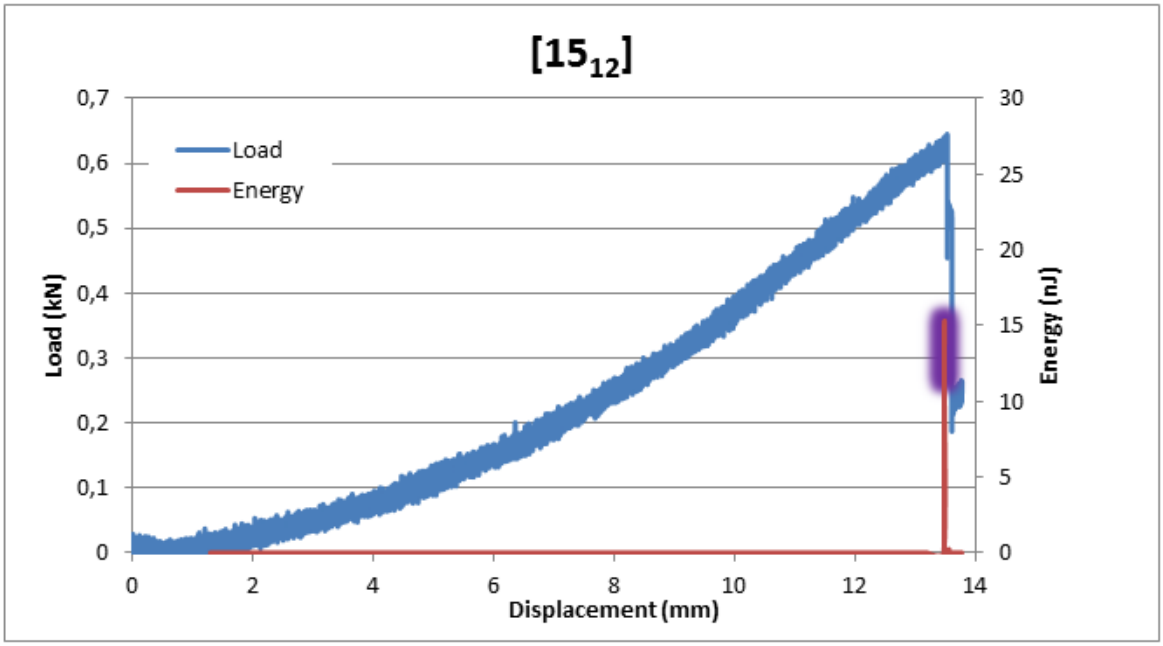

Figure 5.5. Load & energy vs. displacement graph of [5_{12}] configuration laminate.

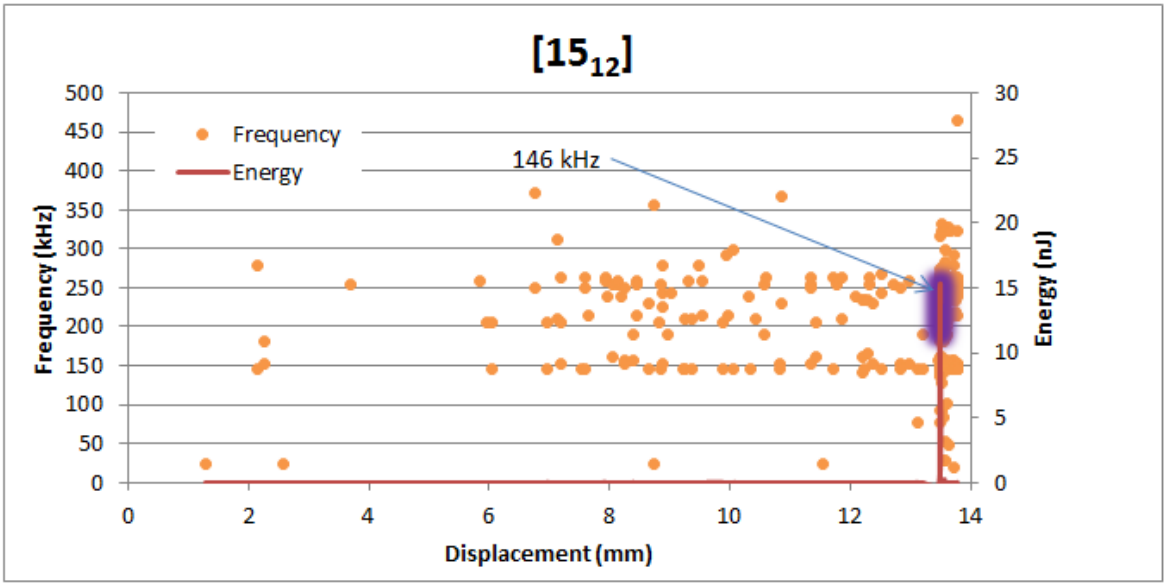

Figure 5.6. Frequency & energy vs. displacement graph of [5_{12}] configuration laminate.

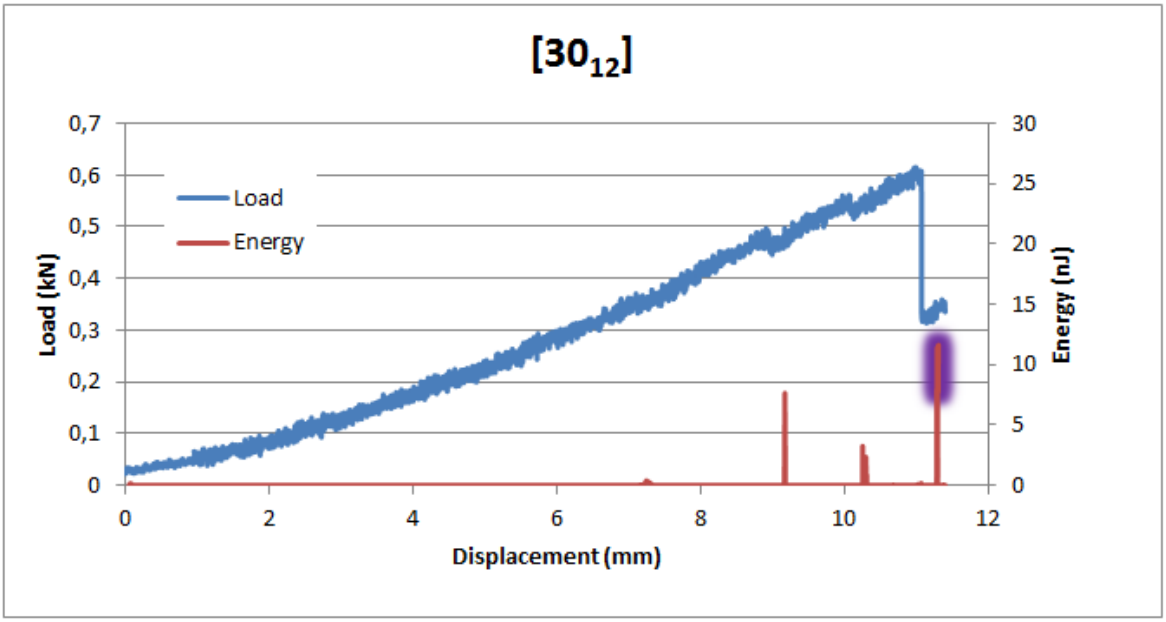

Figure 5.7. Load & energy vs. displacement graph of [30_{12}] configuration laminate.

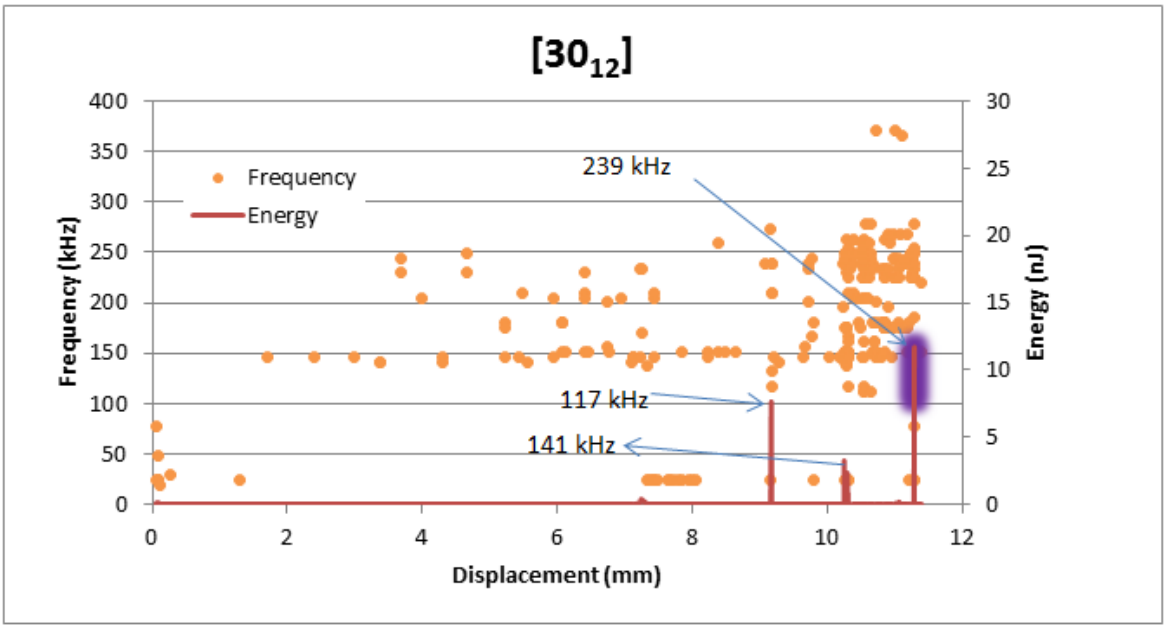

Figure 5.8. Frequency & energy vs. displacement graph of [30_{12}] configuration laminate.

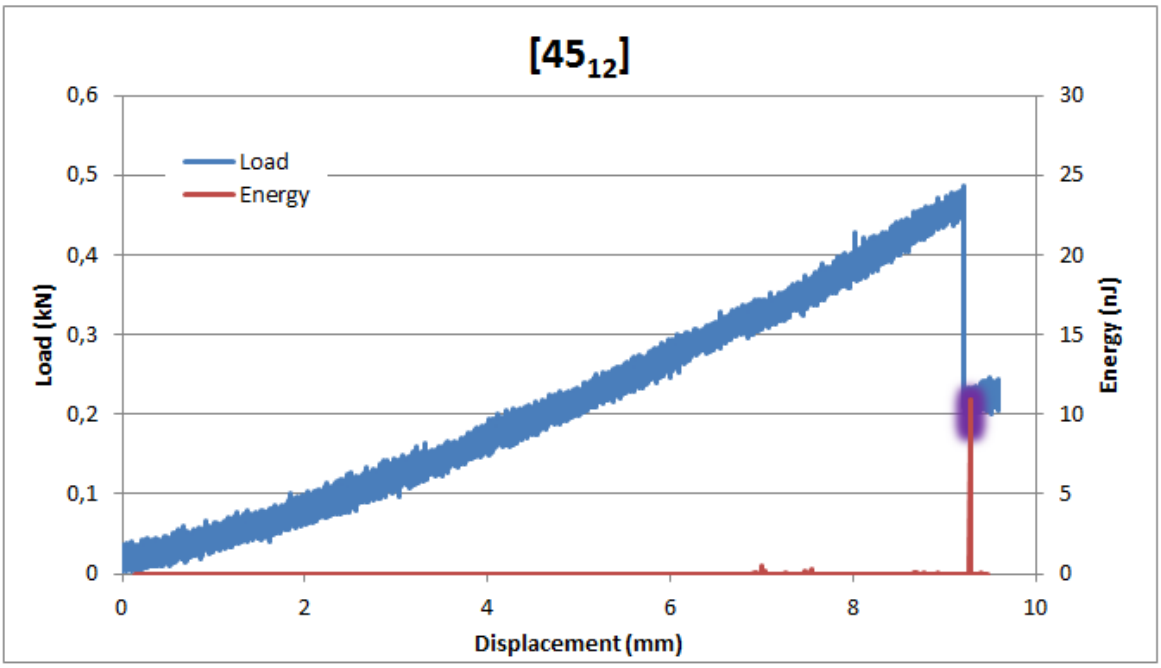

Figure 5.9. Load & energy vs. displacement graph of [45_{12}] configuration laminate.

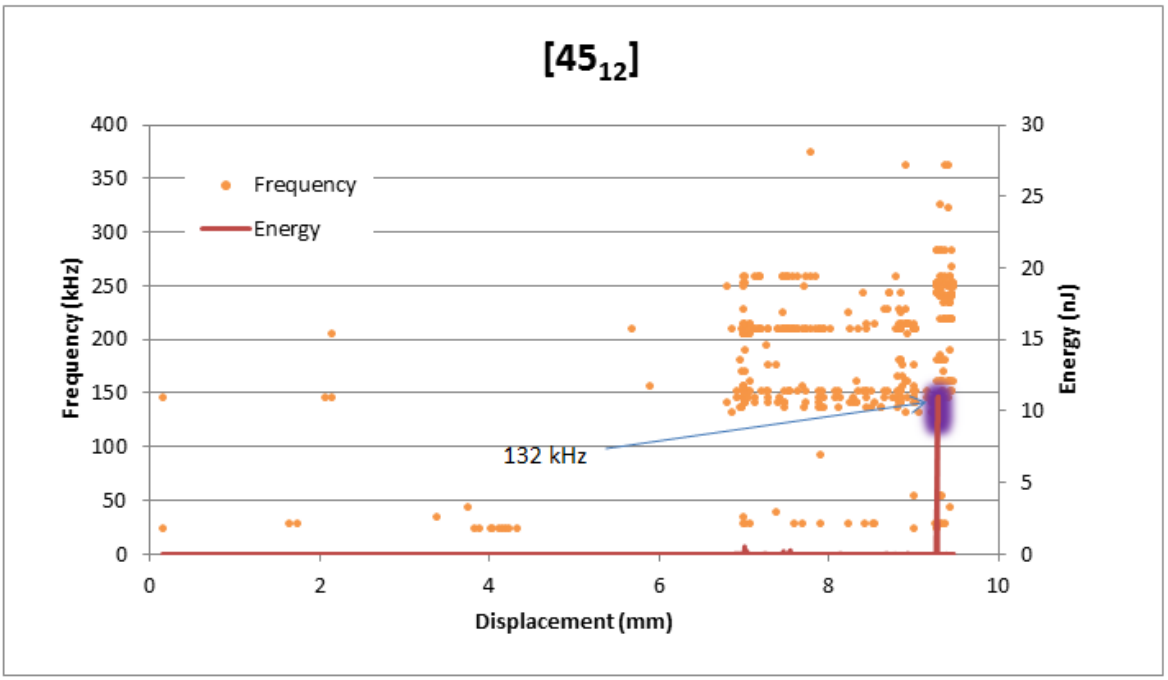

Figure 5.10. Frequency & energy vs. displacement graph of [45_{12}] configuration laminate.

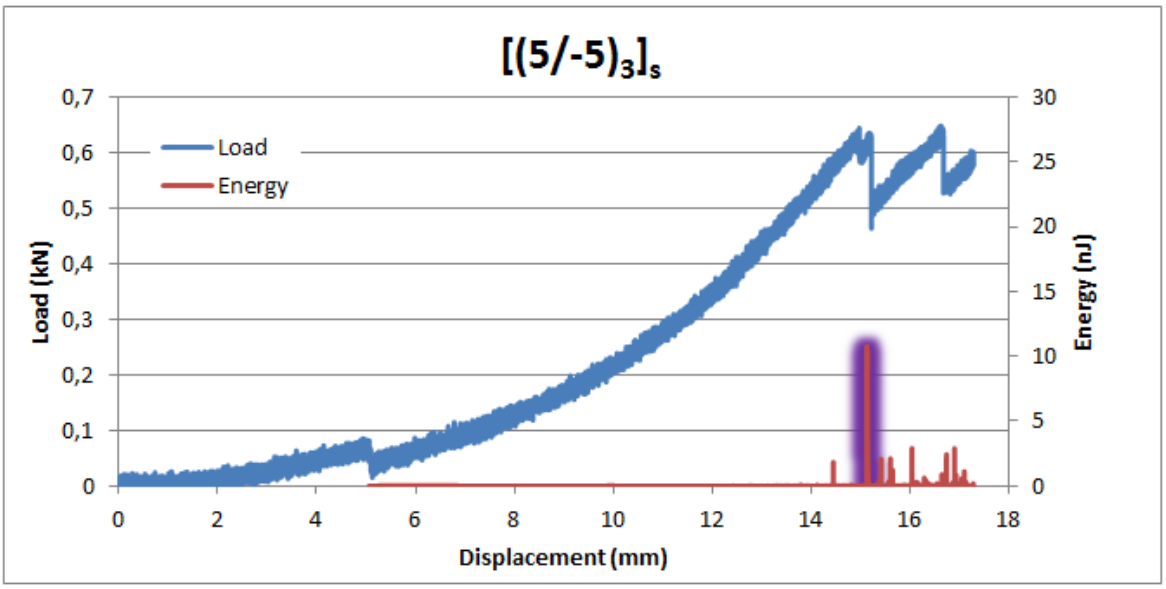

Figure 5.11. Load & energy vs. displacement graph of $[(5/-5)_3]_s$ configuration laminate.

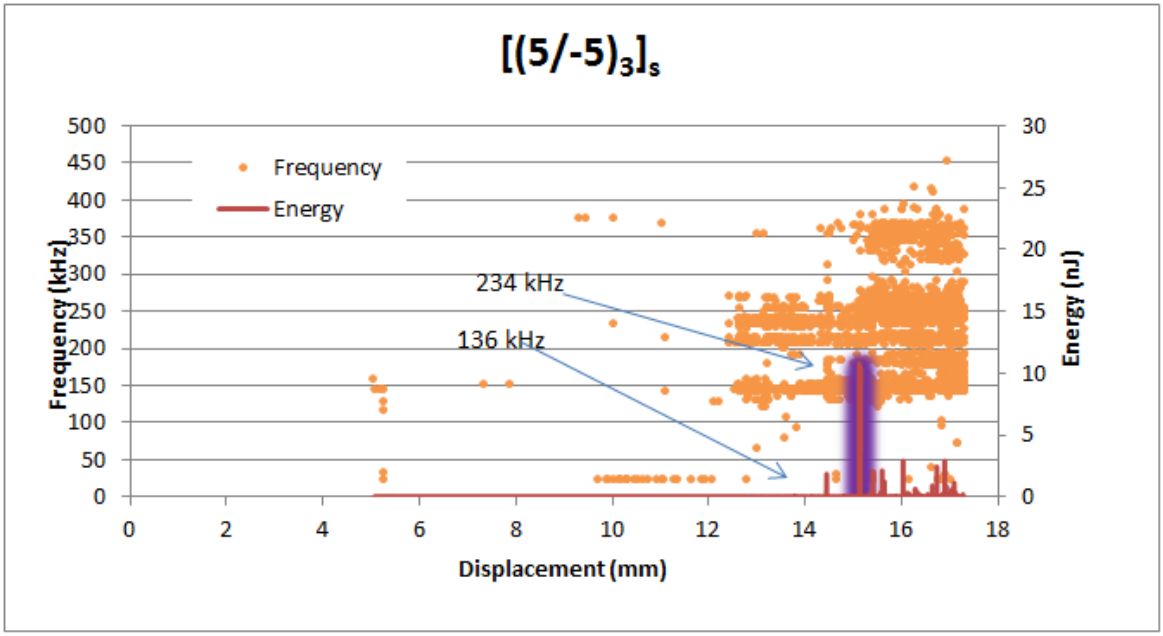

Figure 5.12. Frequency & energy vs. displacement graph of $[(5/-5)_3]_s$ configuration laminate.

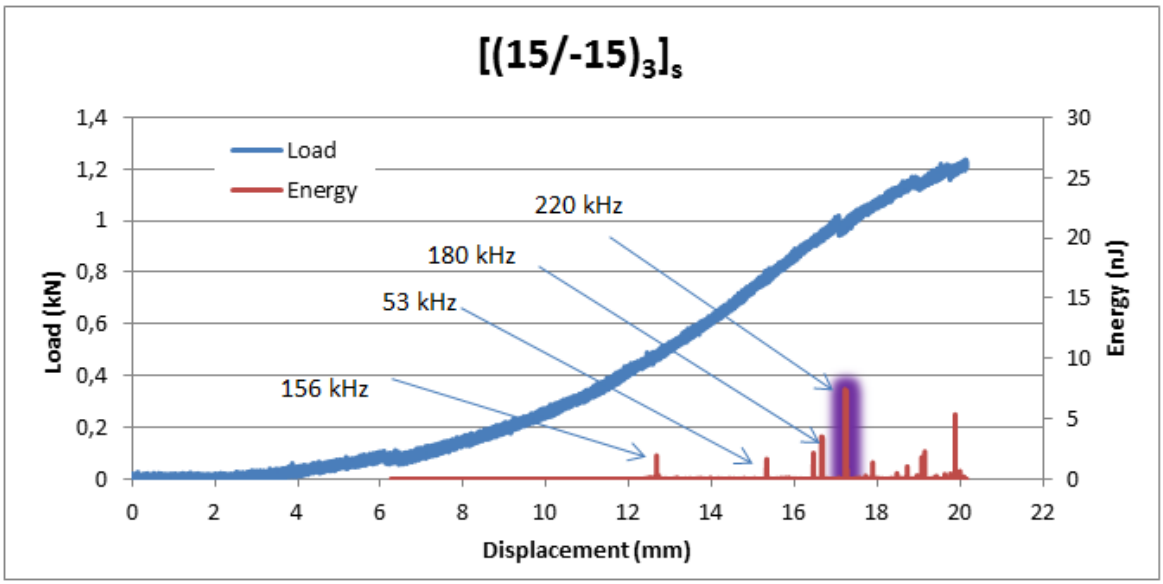

Figure 5.13. Load & energy vs. displacement graph of $[(15/-15)_3]_s$ configuration laminate.

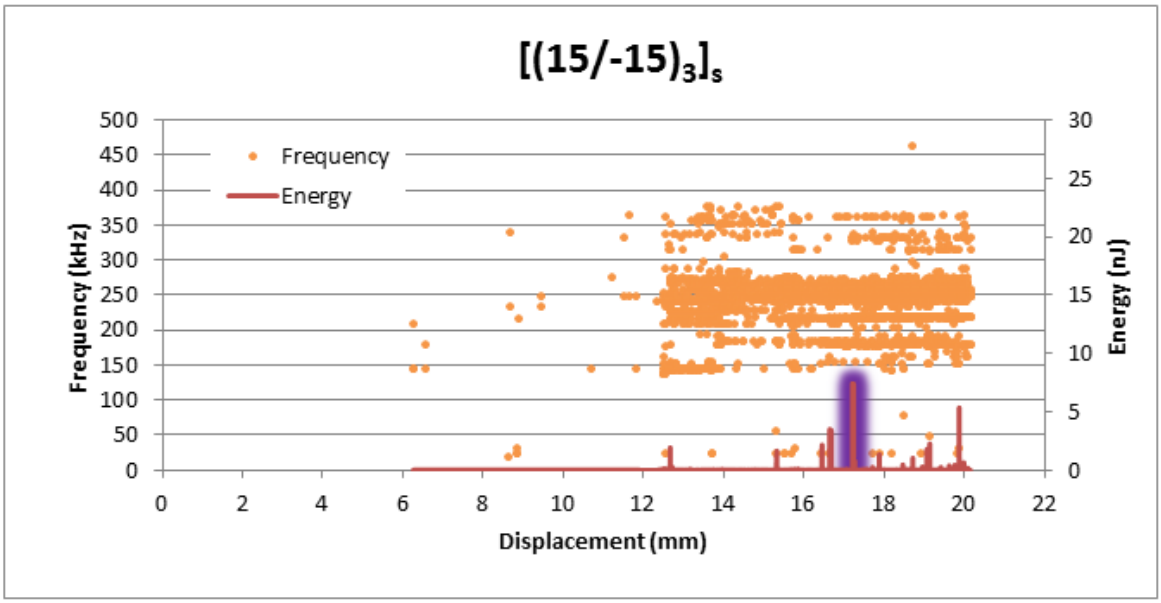

Figure 5.14. Frequency & energy vs. displacement graph of $[(15/-15)_3]_s$ configuration laminate.

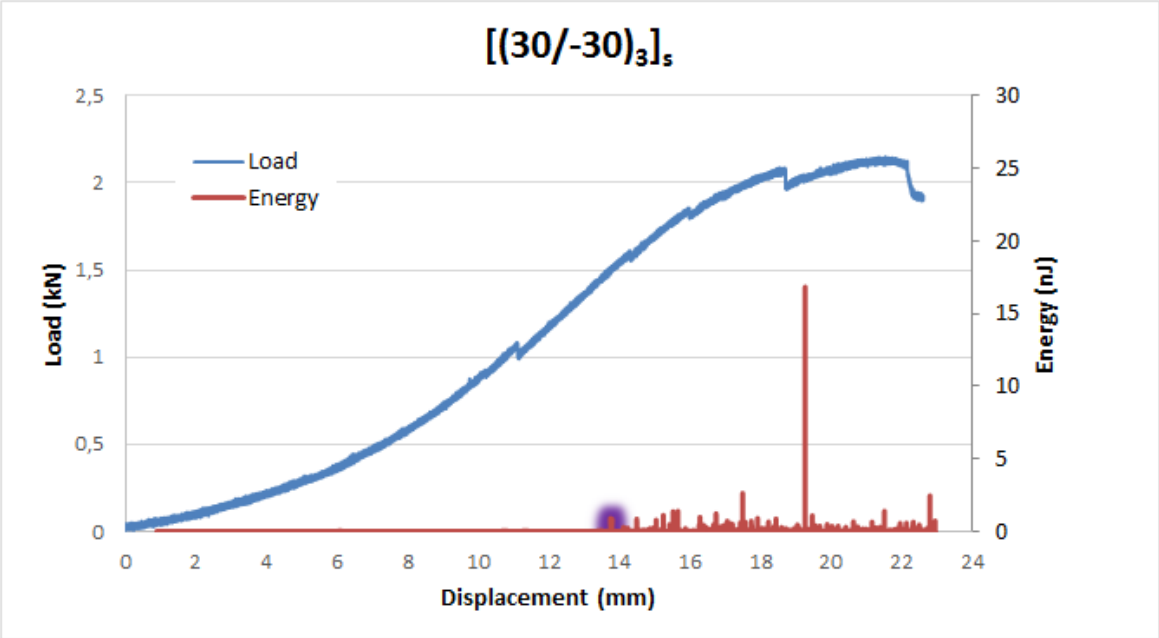

Figure 5.15. Load & energy vs. displacement graph of $[(30/-30)_3]_s$ configuration laminate.

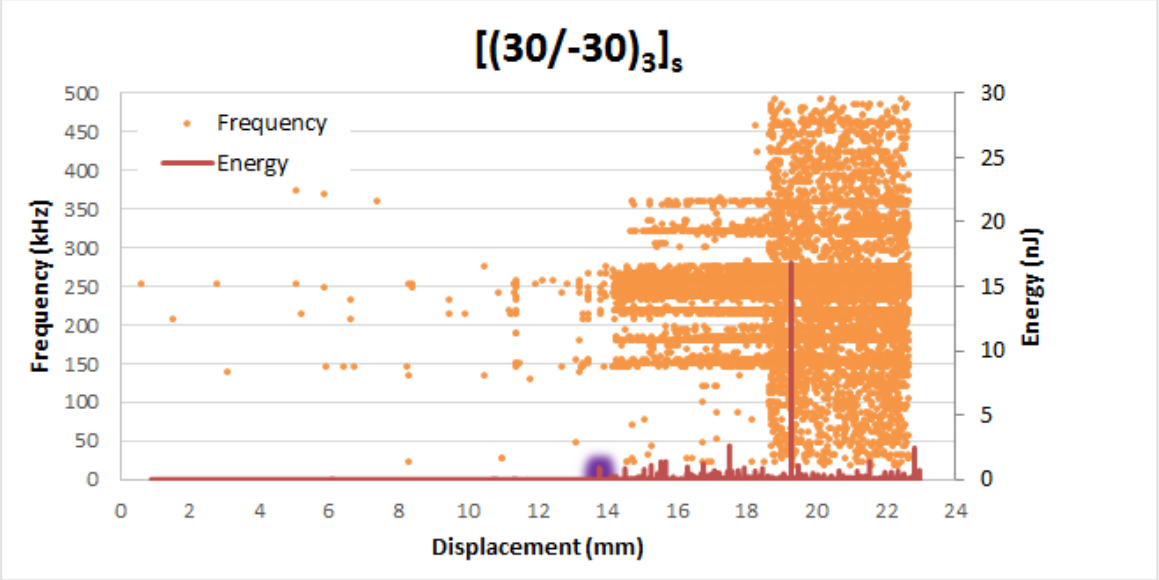

Figure 5.16. Frequency & energy vs. displacement graph of $[(30/-30)_3]_s$ configuration laminate.

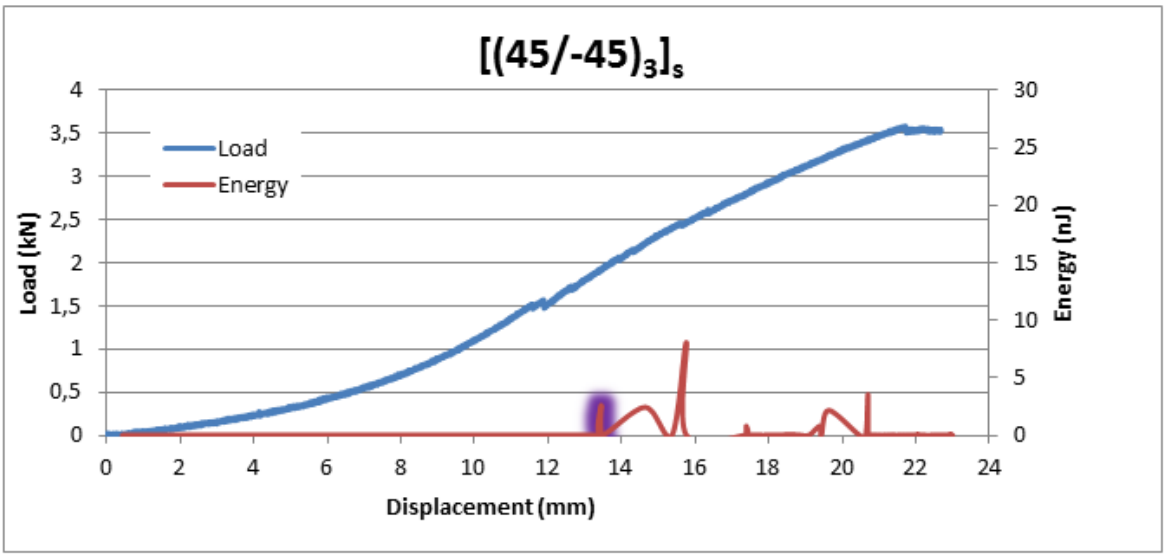

Figure 5.17. Load & energy vs. displacement graph of $[(45/-45)_3]_s$ configuration laminate.

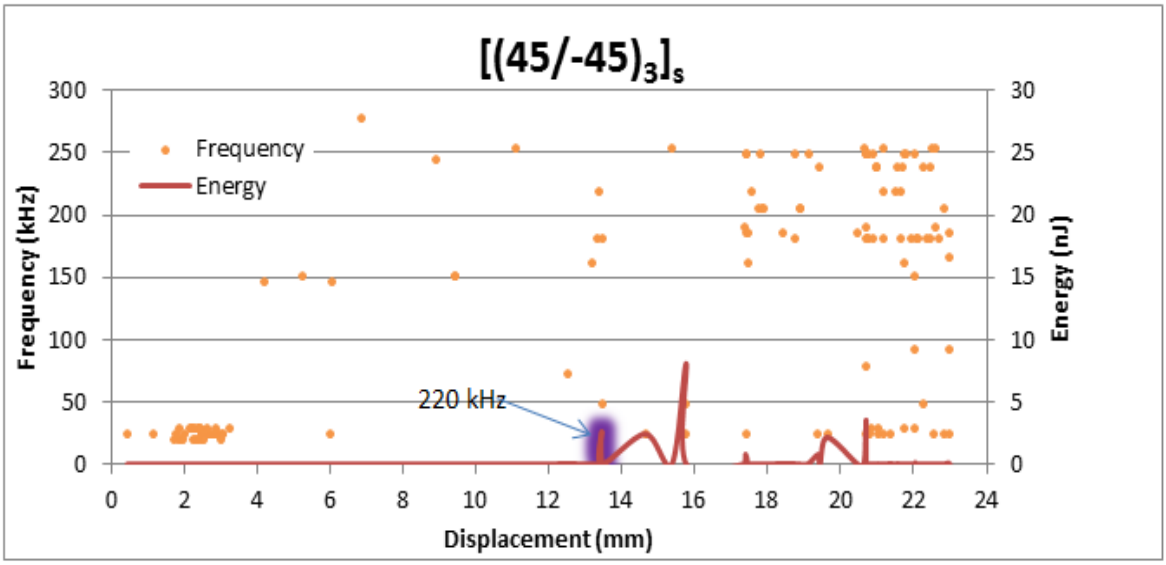

Figure 5.18. Frequency & energy vs. displacement graph of $[(45/-45)_3]_s$ configuration laminate.

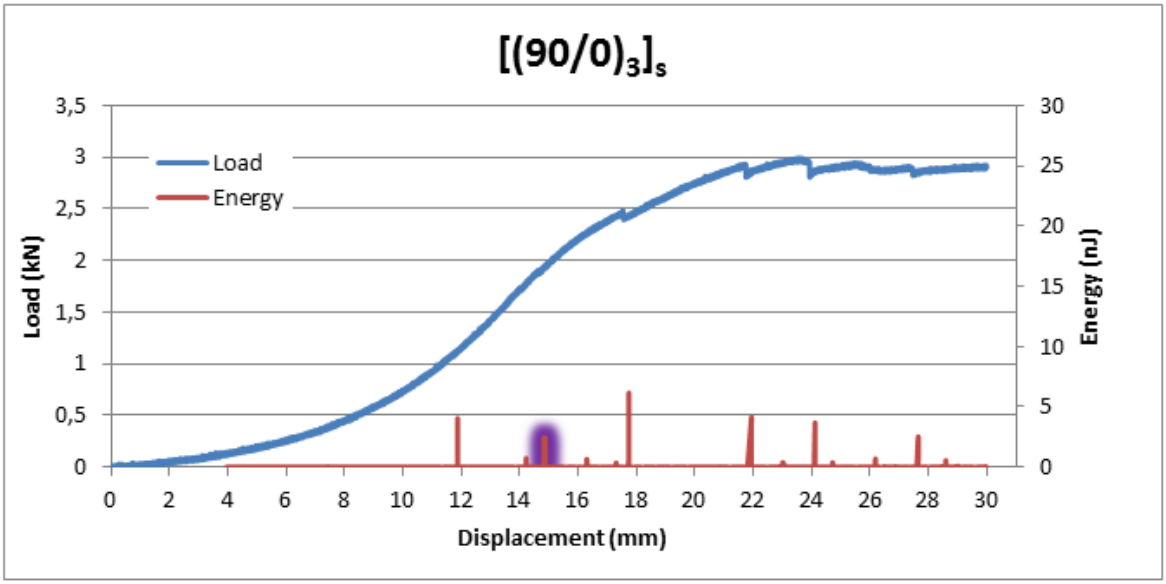

Figure 5.19. Load & energy vs. displacement graph of $[(90/0)_3]_s$ configuration laminate.

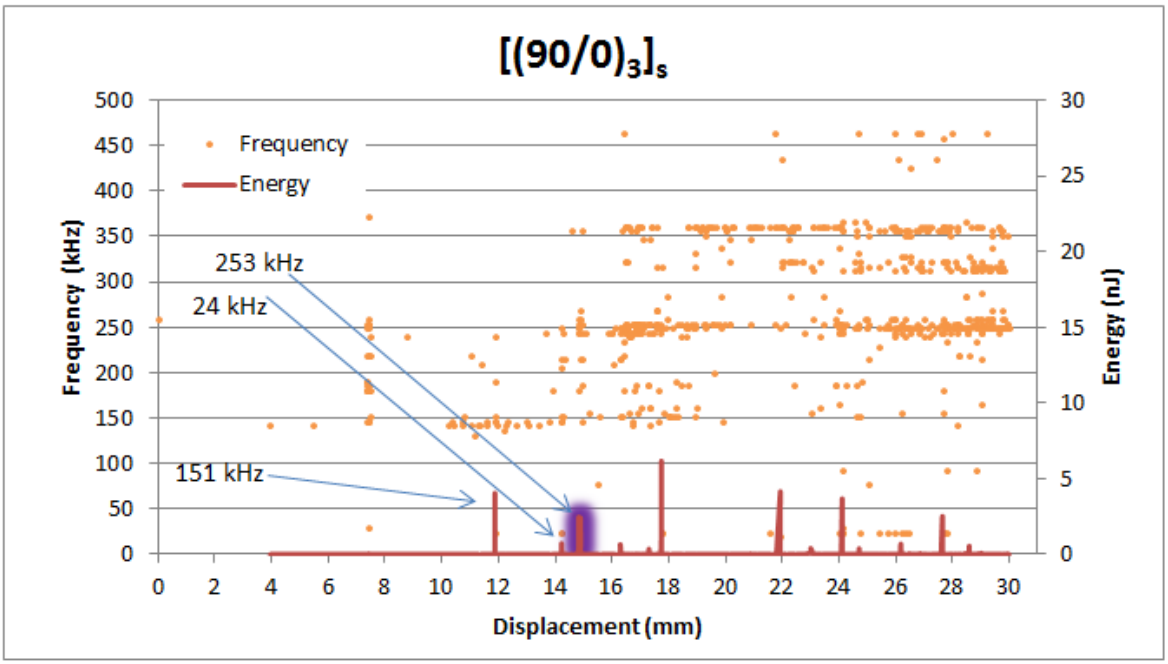

Figure 5.20. Frequency & energy vs. displacement graph of $[(90/0)_3]_s$ configuration laminate.

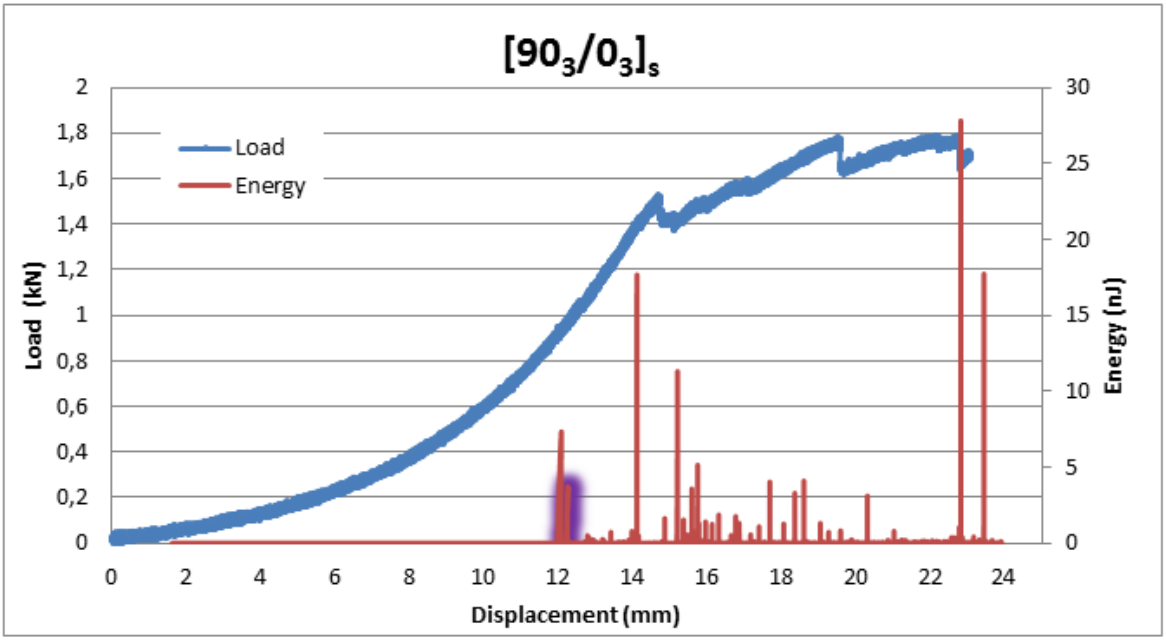

Figure 5.21. Load & energy vs. displacement graph of $[90_3/0_3]_s$ configuration laminate.

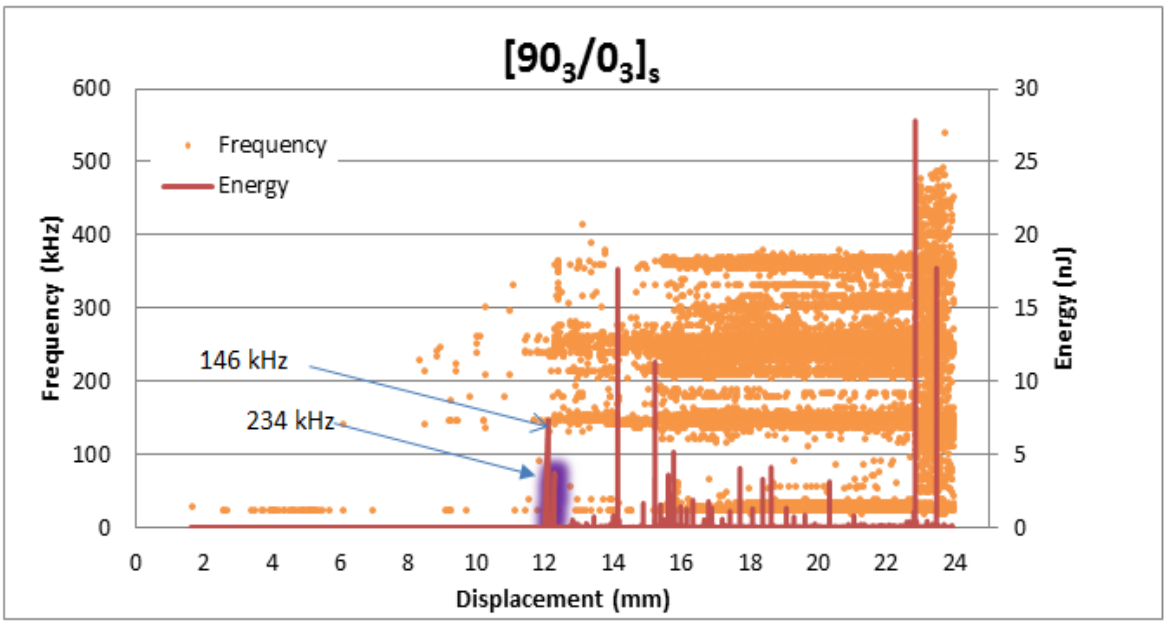

Figure 5.22. Frequency & energy vs. displacement graph of $[90_3/0_3]_s$ configuration laminate.

5.2. Comparison of the Numerical and Experimental Results

5.2.1. Unidirectional laminates

Unidirectional laminates are expected to undergo brittle failure. Occurrence of a brittle catastrophic failure allows one to determine the failure load without performing any acoustic emission monitoring; but AE data are obtained in the present study during testing of the unidirectional specimens to identify and distinguish the emissions coming from edge strip-specimen surface cracks.

In addition to the experimental results, based on the results obtained by the FE model, the failure loads are estimated using the selected composite failure criteria. Figure 5.23 shows a comparison of the experimentally determined failure loads of unidirectional laminated plates, $[\theta_{12}]$, and the predictions obtained using the selected failure criteria. As seen in the figure, the maximum stress and maximum strain criteria predict a different trend from that of the others in the first 10 degrees of the fiber orientation angle θ. At larger angles, predicted load levels begin to look similar and after 20^o the criteria estimate about the same levels for the failure loads.

Table 5.3 tabulates the predicted values of the failure load for the unidirectional laminates. Table 5.4 presents the experimental results for the unidirectional specimens and Table 5.5 gives the percentage errors in the predictions of the failure criteria. As seen in the tables, the largest discrepancies between the experimental results and the predictions occur for $[0_{12}]$ and $[5_{12}]$ configurations. Among the failure criteria, the maximum stress and maximum strain criteria yield the worst predictions with an error up to 43,2 %. The quadratic surfaces criterion returns a relatively good prediction with 20,4 % error. Except maximum stress and maximum strain, the failure criteria predict a decreasing trend for the strength with the increase in the orientation angle, θ. Experiments indicate, however, a decrease in strength for θ = 5°, then increase at 15°, after that a continuous decrease until θ = 45°.

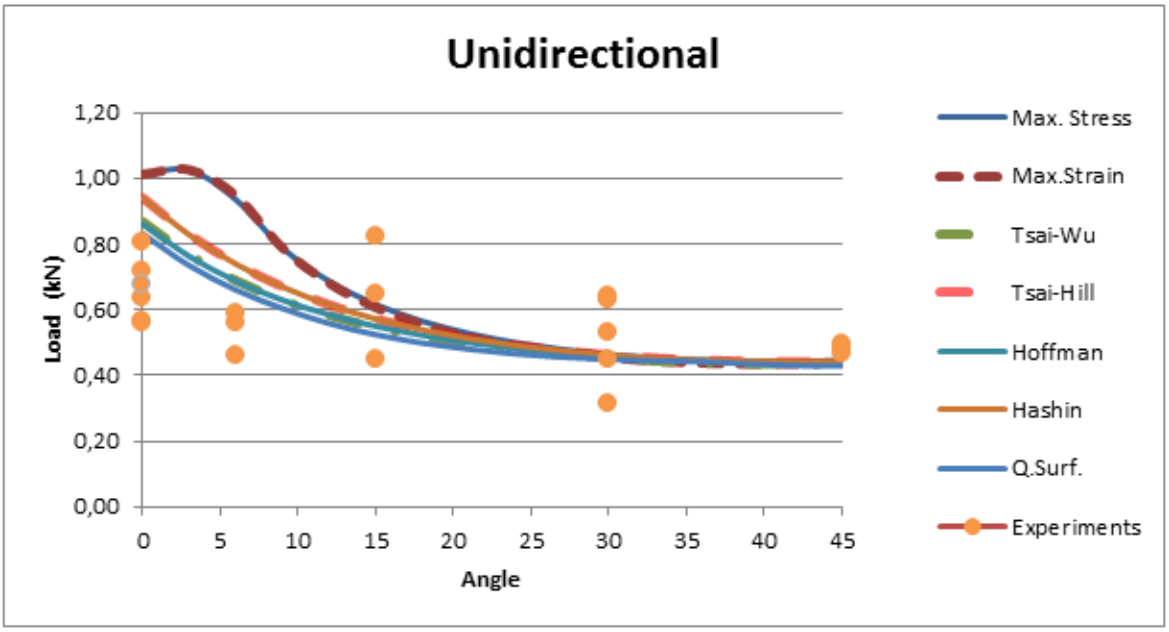

Figure 5. 23. Failure load vs. orientation angle,θ, graph for unidirectional laminates [θ_{12}].

Table 5. 3. Experimental results for unidirectional laminates.

Fiber orientation angle	Failure load(N)	Fiber orientation angle	Failure load (N)
0	562	**30**	628
0	807	**30**	316
0	719	**30**	533
0	635	**30**	451
0	567	**30**	640
0	678	**30(Average)**	514
0 (Average)	661	**45**	468
5	465	**45**	487
5	560	**45**	495
5	591	**45 (Average)**	483
5(average)	539	**Non-stripped specimens(N)**	
15	645	**0**	477
15	825	**15**	447
15	451	**30**	420
15 (Average)	641	**45**	379

Table 5. 4. The failure load levels predicted by the selected criteria for unidirectional laminates, $[\theta_{12}]$.

Angle	Max. Stress	Max.Strain	Tsai-Wu	Tsai-Hill	Hoffman	Hashin	Q.Surf.
0	1012	1012	868	940	861	939	831
3	1026	1026	767	829	762	828	734
6	935	947	689	740	687	739	660
9	788	787	629	670	630	669	604
12	687	681	583	615	585	615	558
15	616	607	547	572	550	572	524
18	565	554	518	539	522	539	499
21	528	517	495	512	500	513	480
24	500	489	478	491	483	492	466
27	480	469	463	475	469	476	456
30	465	454	452	462	457	463	449
33	454	444	444	453	449	453	445
36	447	438	439	447	443	447	443
39	444	435	435	443	440	443	435
42	443	436	434	442	438	442	431
45	446	440	436	444	440	444	429

Table 5.5. Average error percentages of failure criteria results of unidirectional orientations according to related experiments.

	Max. Stress	Max.Strain	Tsai-Hill	Tsai-Wu	Hoffman	Hashin	Q.Suf.
Angle, θ	**Error**	**Error**	**Error**	**Error**	**Error**	**Error**	**Error**
0(average)	34.7%	34.7%	29.6%	23.8%	29.6%	23.2%	20.4%
5(average)	42.6%	43.3%	22.1%	27.5%	21.9%	27.4%	18.7%
15(Average)	-3.9%	-5.6%	-11.9%	-17.2%	-11.9%	-16.5%	-22.2%
30(Average)	-10.6%	-13.1%	-11.1%	-13.6%	-11.0%	-12.3%	-14.4%
45(Average)	-8.3%	-9.9%	-9.0%	-10.7%	-8.9%	-9.9%	-12.56%

Figures 5.24 to 5.30 show the FEM-based predictions of each failure criteria and experiment results for the unidirectional specimens.

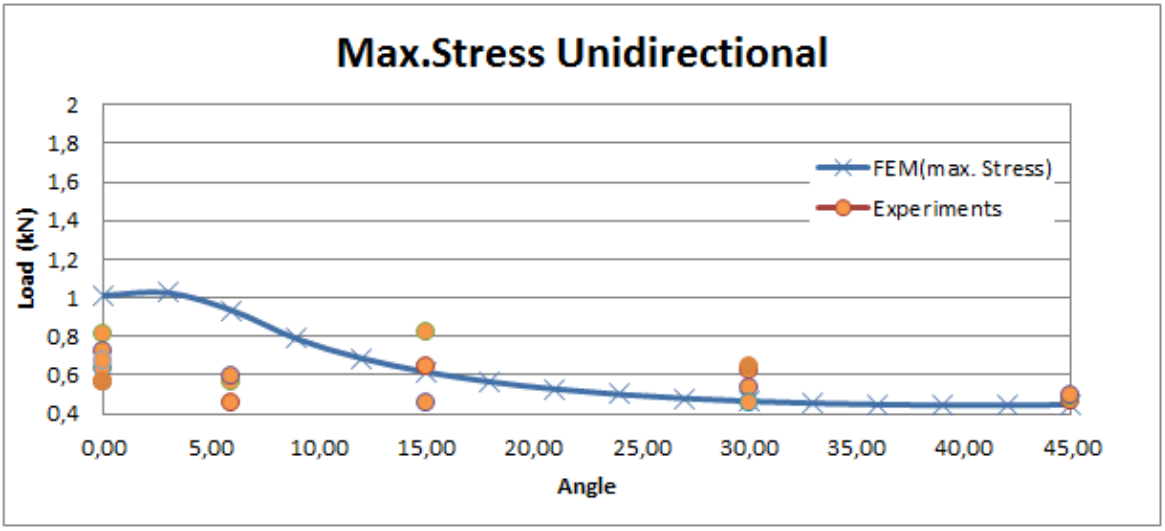

Figure 5. 24. Comparison of the FEM predictions obtained by the maximum stress criterion with the experimental results for unidirectional [θ_{12}] specimens.

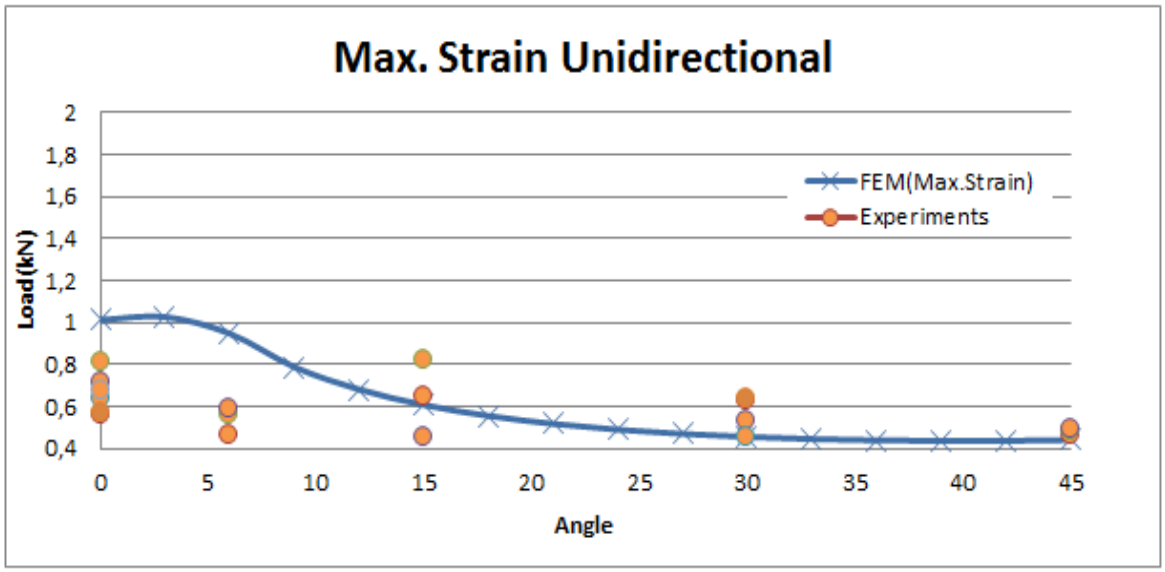

Figure 5.25. Comparison of the FEM predictions obtained by the maximum strain criterion with the experimental results for unidirectional [θ_{12}] specimens.

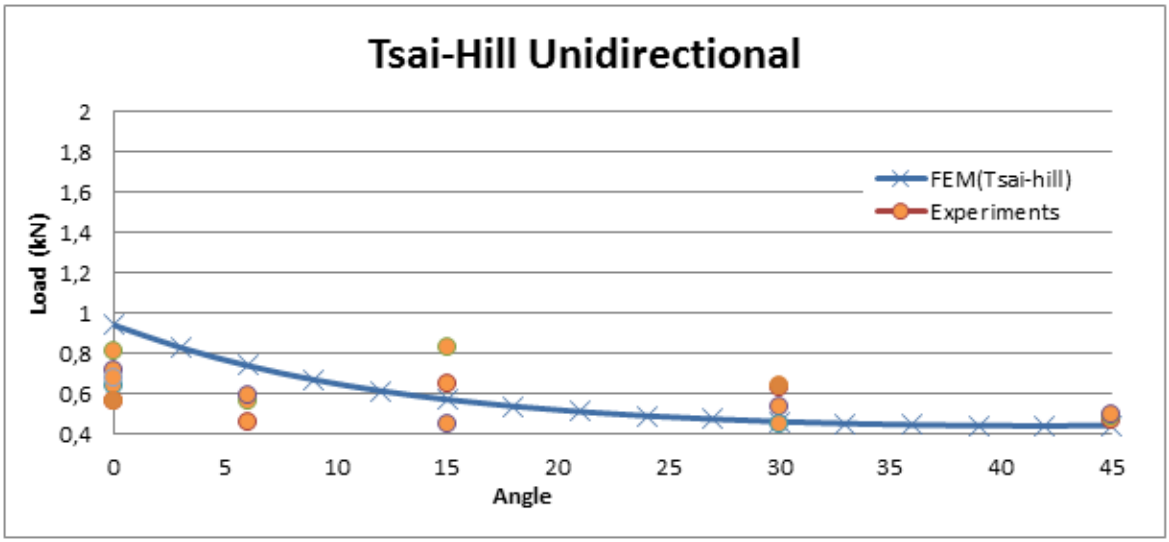

Figure 5.26. Comparison of the FEM predictions obtained by the Tsai-Hill criterion with the experimental results for unidirectional [θ_{12}] specimens.

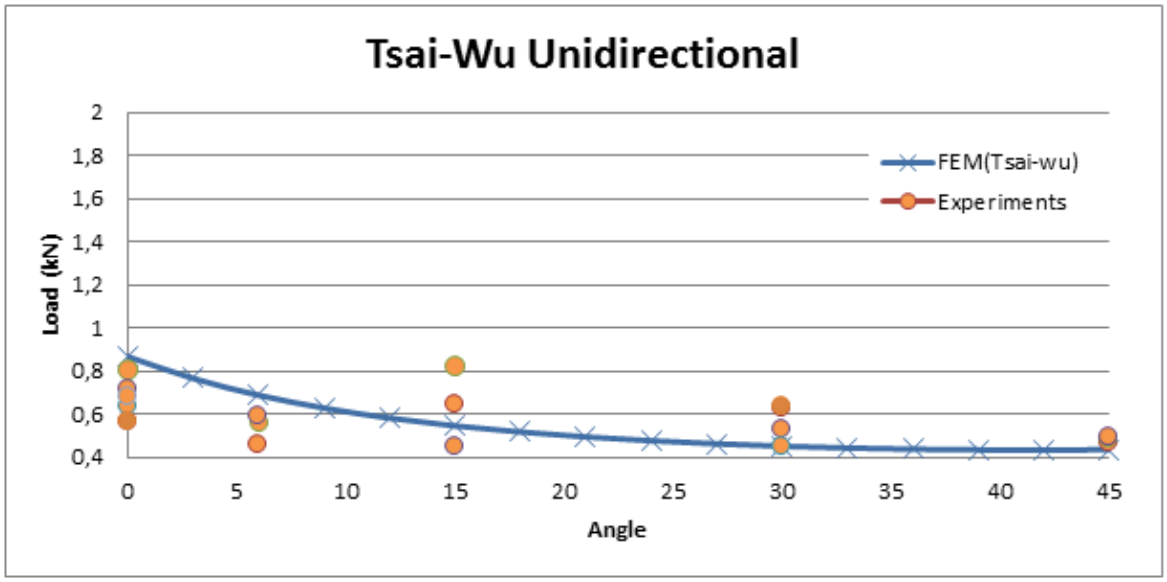

Figure 5.27. Comparison of the FEM predictions obtained by the Tsai-Wu criterion with the experimental results for unidirectional [θ_{12}] specimens.

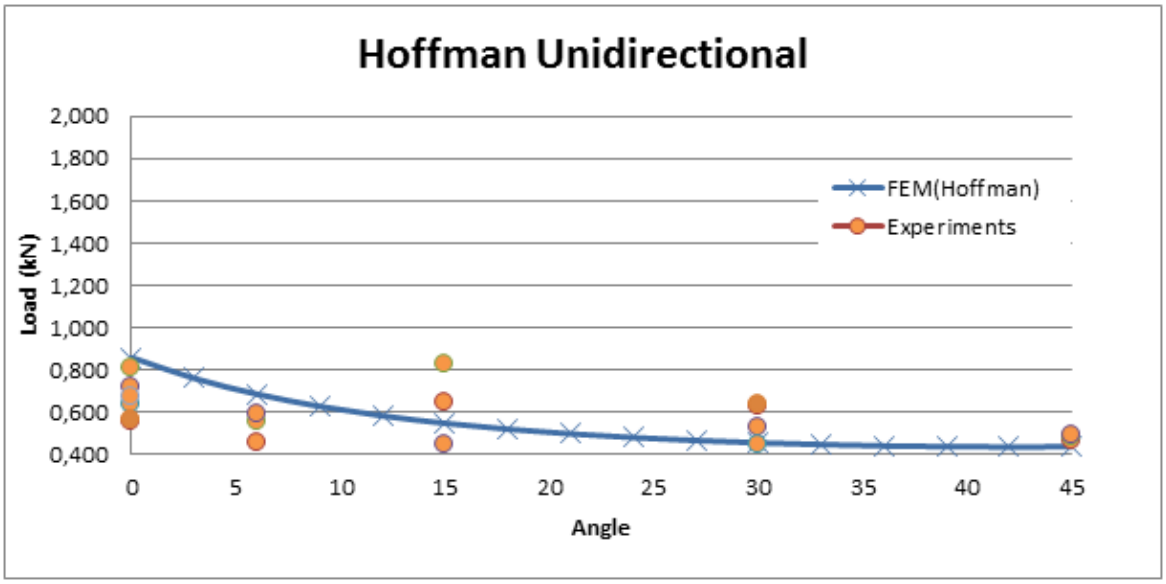

Figure 5.28. Comparison of the FEM predictions obtained by the Hoffman criterion with the experimental results for unidirectional [θ_{12}] specimens.

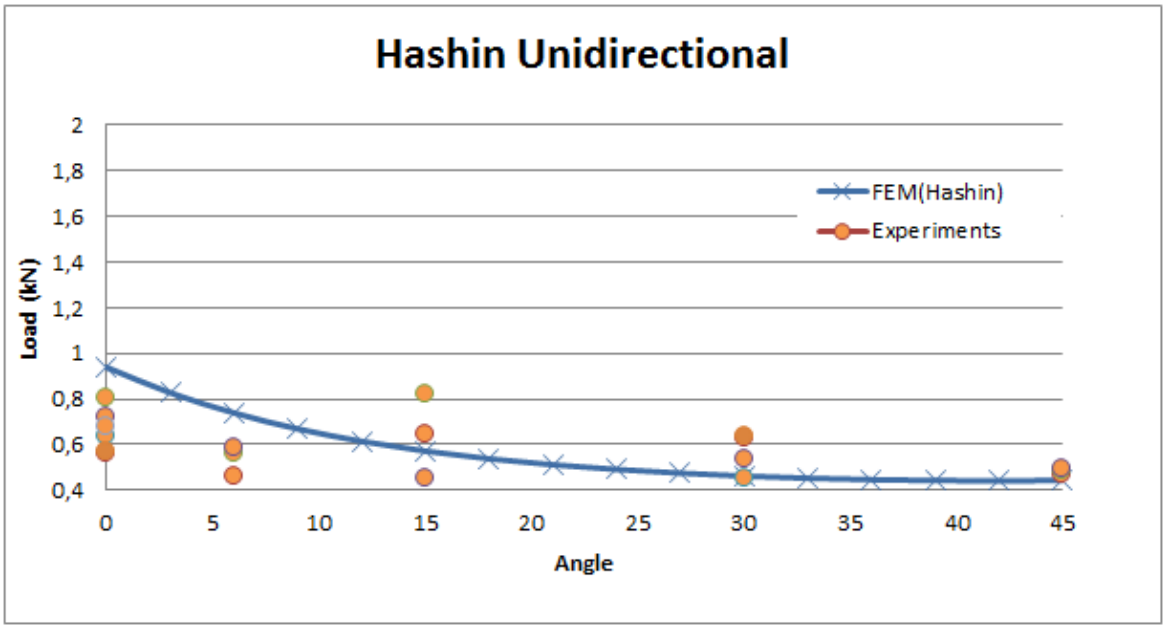

Figure 5.29. Comparison of the FEM predictions obtained by the Hashin criterion with the experimental results for unidirectional [θ_{12}] specimens.

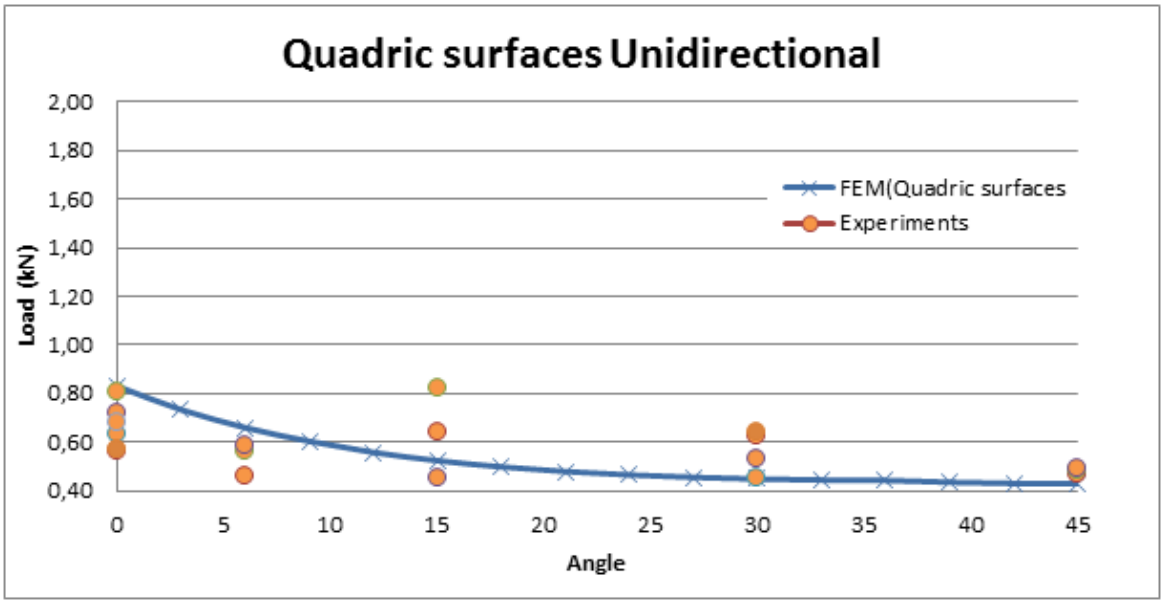

Figure 5.30. Comparison of the FEM predictions obtained by the quadric surfaces criterion with the experimental results for unidirectional [θ12] specimens.

5.2.2. Symmetric-Balanced laminates, $[(\theta/-\theta)_3]_s$

Table 5.6 presents the experimental results. The scatter in the experimental results is lower compared to the unidirectional specimen results. This may be attributed to the sensitivity of the matrix dominated transverse strength to manufacturing defects, which has much more bearing on unidirectional laminates. The highest strength is obtained for $[(45°/-45°)_3]_s$ laminates, while $[(5/-5)_3]_s$ has the lowest strength.

Table 5.7 tabulates the values of the failure load predicted by the selected failure criteria based on the FE results for symmetric-balanced laminates. The average errors of related configurations are given in Table 5.8. Figure 5.31 gives a comparison of the predictions and the experimental results for symmetric-balanced laminates. According to the experiments, strength of the material decreases for $\theta=5^0$ and then increases continuously.

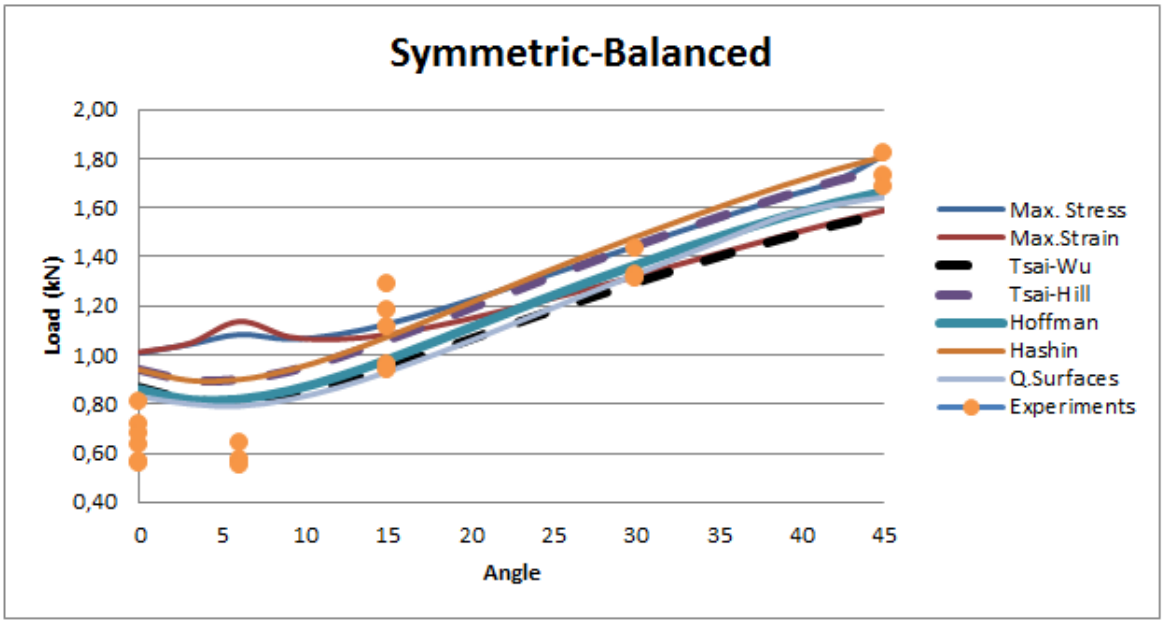

Figure 5.31. Failure load vs. orientation angle, θ, graph for symmetric-balanced laminates $[(\theta/-\theta)_3]_s$.

Table 5.6. Experimental results for symmetric-balanced laminates, [(θ/-θ)3]s.

Fiber Orientation Angle	Failure Load (N)
5/-5	576
5/-5	567
5/-5	551
5/-5	639
5/-5(average)	**583**
15/-15	1292
15/-15	1183
15/-15	1112
15/-15	940
15/-15	960
15/-15(Average)	**1097**
30/-30	1436
30/-30	1330
30/-30	1314
30/-30(Average)	**1360**
45/-45	1733
45/-45	1822
45/-45	1686
45/-45(Average)	**1747**
Non-stripped specimens(N)	
30/-30	1360
45/-45	1747

Table 5.7. The failure load levels in Newton predicted by the selected criteria for symmetric-balanced laminates, $[(\theta/-\theta)_3]_s$.

Angle	Max. Stress	Max.Strain	Tsai-Wu	Tsai-Hill	Hoffman	Hashin	Q.Surf.
0	1008	1012	868	940	861	939	831
3	1043	1047	818	898	818	896	801
6	1084	1137	813	900	820	900	792
9	1065	1074	839	934	855	938	818
12	1085	1064	888	991	912	1000	868
15	1127	1084	950	1062	982	1075	933
18	1183	1120	1018	1139	1060	1158	1007
21	1245	1165	1089	1219	1140	1242	1086
24	1311	1215	1160	1297	1218	1325	1166
27	1378	1268	1229	1373	1295	1405	1248
30	1445	1322	1296	1447	1368	1482	1329
33	1512	1377	1360	1517	1438	1556	1410
36	1579	1433	1421	1585	1504	1627	1490
39	1645	1488	1478	1649	1565	1694	1569
42	1708	1541	1530	1708	1620	1755	1614
45	1816	1590	1574	1760	1667	1809	1643

Table 5.8. Average error percentages of failure criteria results of symmetric-balanced configurations according to related experiments.

	Max.Stress	Max. Strain	Tsai-Hill	Tsai-Wu	Hoffman	Hashin	Q.Surf.
angle	Error	Error	Error	Error	Error	Error	Error
5/-5	46.17%	48.69%	28.23%	35.16%	28.90%	35.20%	26.40%
15/-15	2.63%	-1.28%	-13.08%	-3.37%	-11.74%	-2.52%	-17.69%
30/-30	5.83%	-2.87%	5.97%	-4.93%	8.27%	0.60%	-2.31%
45/-45	3.82%	-9.88%	-3.04%	-7.20%	0.78%	-2.17%	-6.33%

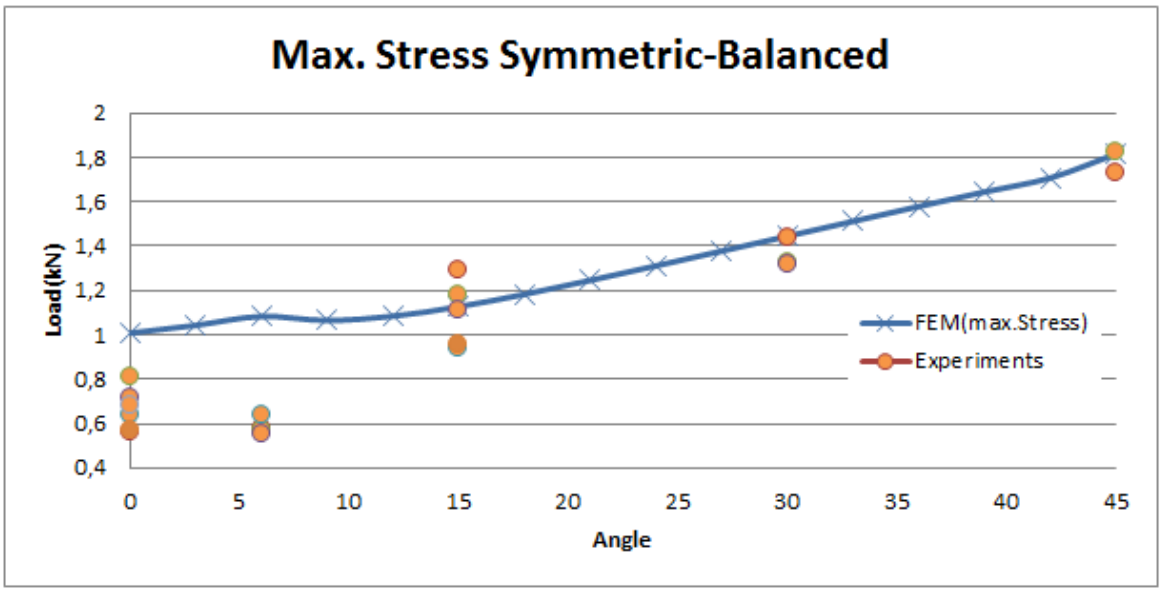

Figure 5.32. Comparison of the FEM predictions obtained by the maximum stress criterion with the experimental results for symmetric balanced $[(\theta/-\theta)_3]_s$ laminates.

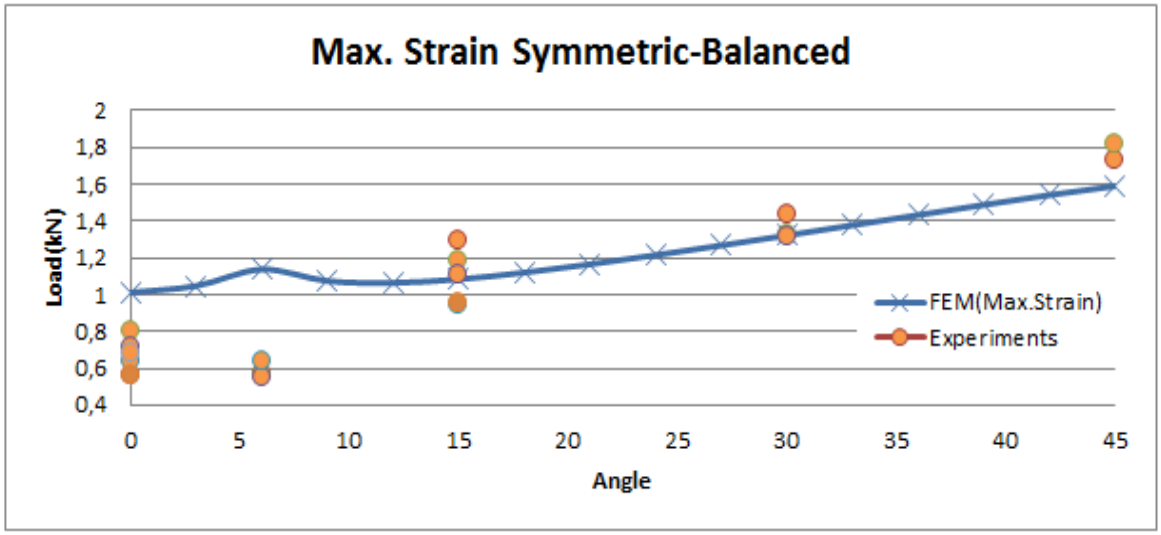

Figure 5.33. Comparison of the FEM predictions obtained by the maximum strain criterion with the experimental results for symmetric balanced $[(\theta/-\theta)_3]_s$ laminates.

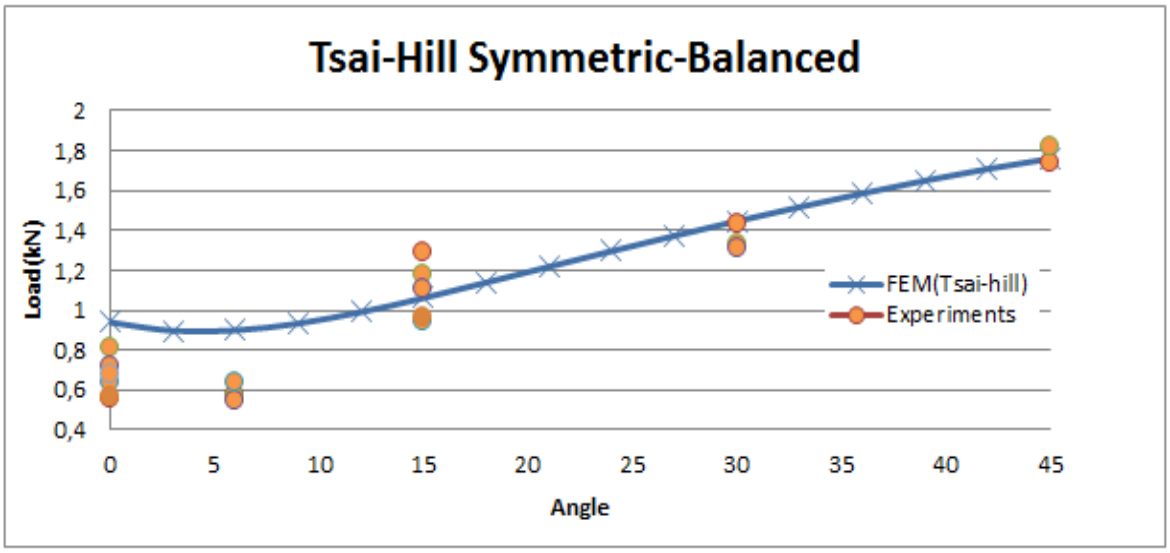

Figure 5.34. Comparison of the FEM predictions obtained by the Tsai-Hill criterion with the experimental results for symmetric balanced $[(\theta/-\theta)_3]_s$ laminates.

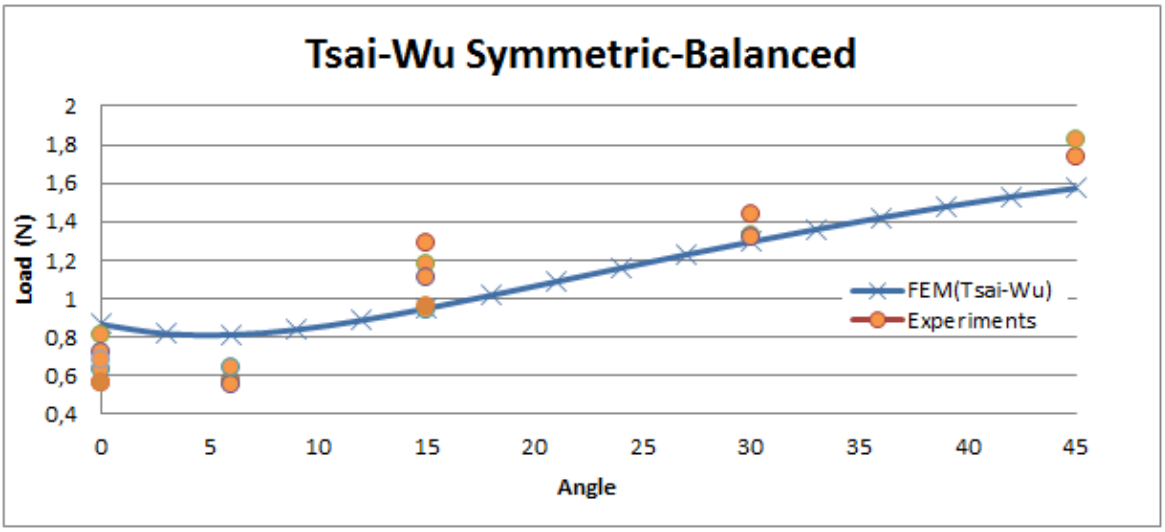

Figure 5.35. Comparison of the FEM predictions obtained by the Tsai-Wu criterion with the experimental results for symmetric balanced $[(\theta/-\theta)_3]_s$ laminates.

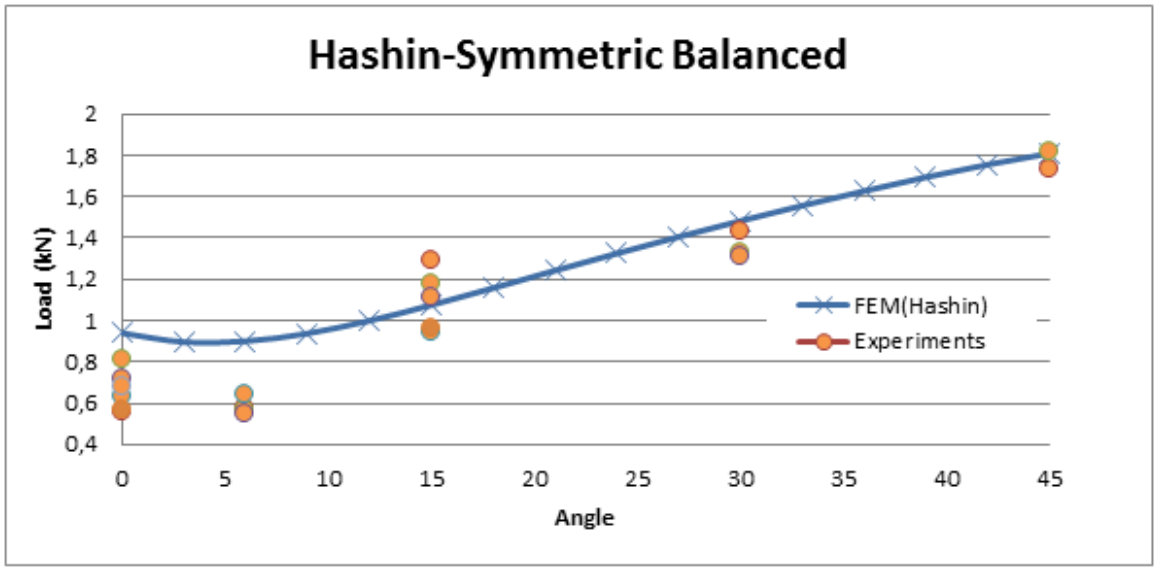

Figure 5.36. Comparison of the FEM predictions obtained by the Hoffman criterion with the experimental results for symmetric balanced $[(\theta/-\theta)_3]_s$ laminates.

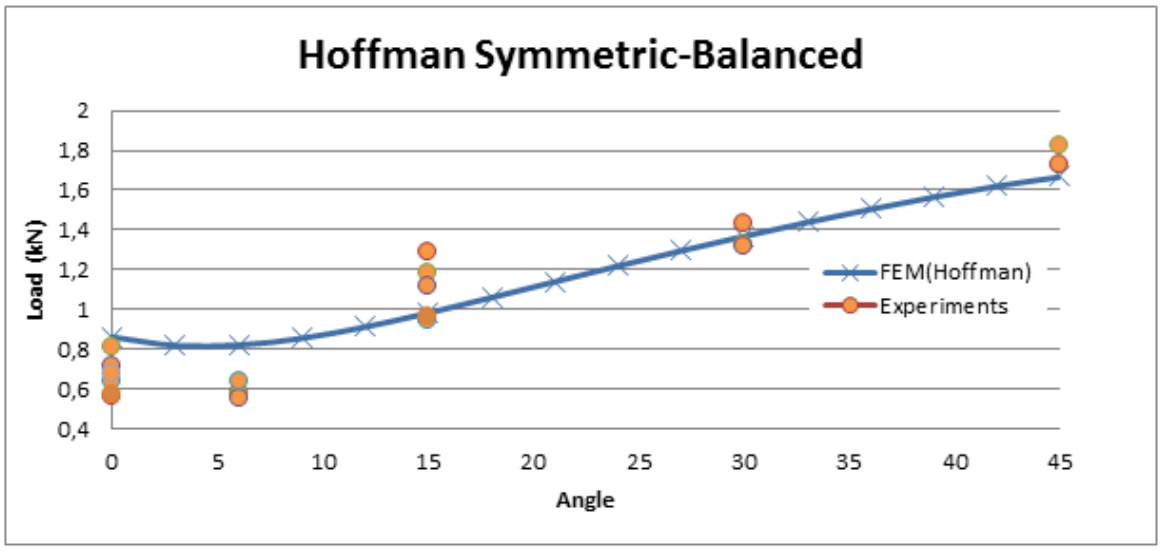

Figure 5.37. Comparison of the FEM predictions obtained by the Hashin criterion with the experimental results for symmetric balanced $[(\theta/-\theta)_3]_s$ laminates.

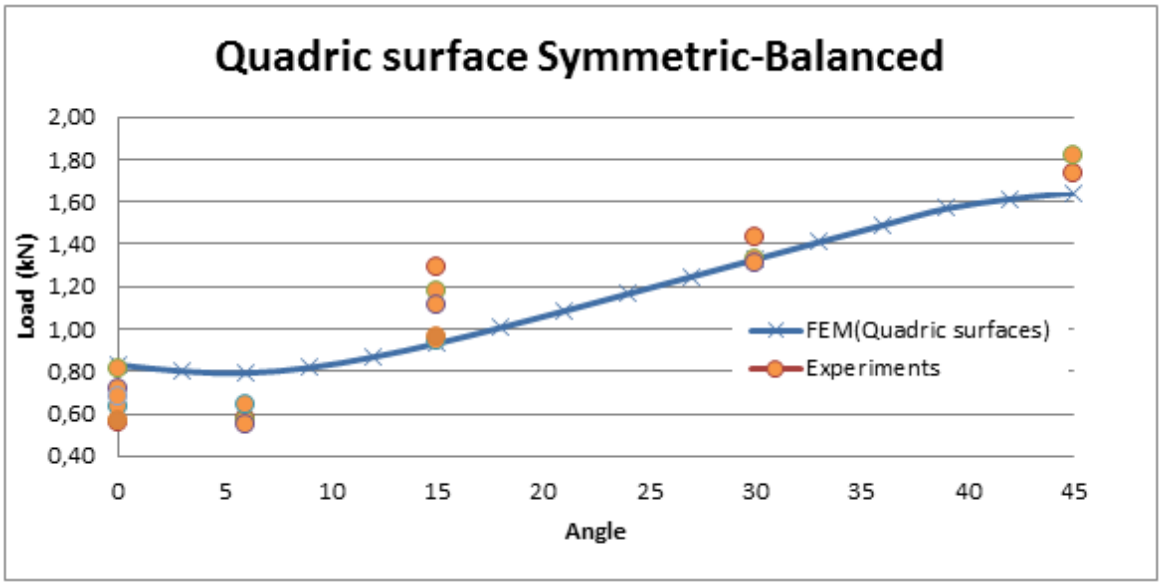

Figure 5.38. Comparison of the FEM predictions obtained by the Quadric surfaces criterion with the experimental results for symmetric balanced $[(\theta/-\theta)_3]_s$ laminates.

5.3. Other Layups

Laminates having $[(90/0)_3]_s$ and $[90_3/0_3]_s$ layup sequences are also tested and FEM-based predictions of the criteria, experimental results, and percentage of error related to all criteria are tabulated in Tables 5.9, 5.10, and 5.11 respectively. Experiments show that the first-ply failure strength of $[(90/0)_3]_s$ laminate is slightly higher than $[90_3/0_3]_s$ laminate in contrast to the predictions of the criteria. However, the ultimate strength of $[(90/0)_3]_s$ laminate is much higher as Figures 5.19 and 5.20 indicate.

Table 5.9. Predictions of failure criteria $[(90/0)_3]_s$ and $[90_3/0_3]_s$ configurations.

Configurations	Max stress	Max strain	Tsai-Wu	Tsai-Hill	Hoffman	Hashin	Q.Surf.
$[(90/0)_3]_s$	1232	1353	1232	1232	1232	1232	1208
$[90_3/0_3]_s$	1251	1374	1236	1251	1233	1251	1215

Table 5.10. Experimental results of $[(90/0)_3]_s$ and $[90_3/0_3]_s$ configurations.

Configurations	exp #1(N)	exp #2(N)	exp #3(N)	Average(N)	Non-stripped specimen
$[(90/0)_3]_s$	1074	1124	1044	1081	1900
$[90_3/0_3]_s$	776	1047	1223	1015	1070

Table 5.11. Average error percentages of all failure criteria.

	Error%	Error%	Error%	Error%	Error%	Error%	Error%
configuration	Max Stress	Max Strain	Tsai Wu	Tsai-Hill	Hoffman	Hashin	Q.Surf.
Average error%	12.29%	20.14%	12.30%	12.29%	12.27%	12.27%	10.53%
Average error%	18.85%	26.11%	17.87%	18.85%	17.65%	18.84%	16.43%

CONCLUSIONS AND FUTURE WORK

In this study, failure behavior of laminated composite plates under anticlastic bending is investigated. Carbon-fiber-reinforced epoxy is selected as the material of the specimens. First-ply failure load is determined by using acoustic emission monitoring (AEM). Reinforcing strips are glued to the edges of the specimens to avoid premature failure by delamination. In order to differentiate the noise signals emitted by the bonded reinforcing strips from the signals resulting from initiation of damage within the specimen, additional tests are conducted without the reinforcing strips and the frequency contents of the noises are examined. Overwhelming amount of the noise signals is detected in the frequencies between 110 kHz and 170 kHz. An energy-based method is employed to detect the first-ply-failure. The time of the first signal which yields the peak energy is considered as the first-ply failure initiation time. Using the time vs. load diagram obtained from the test machine, the corresponding failure load is found. The frequency of the detected signal for the initiation of the failure is generally between 200 kHz and 300 kHz. This frequency range corresponds to fiber-matrix debonding failure mechanism as reported in the literature. This means that the detected first-ply failure mode is a static failure mode, not delamination.

A finite element model is developed to carry out the structural analysis of the specimen under anticlastic bending. Selected failure criteria are then employed to predict the failure load. The predictions of the failure criteria generally show a good agreement with the experimental results for the symmetric balanced, cross-ply, and the other selected multi-directional configurations. But for unidirectional cases, especially for $[0_{12}]$ and $[5_{12}]$ configurations, predictions show larger discrepancies. They all overestimate the strengths of $[0_{12}]$ and $[5_{12}]$ configurations by 23% to 43%. There are also differences in predicted failure trends for unidirectional laminates $[\theta_{12}]$. Maximum stress and maximum strain criteria predict the strength of $[3]_{12}$ higher than that of $[0]_{12}$, while the others predict the highest strength for $[0]_{12}$, then continuously decreasing strength up to 45°. The latter trend conforms to the experimental results better. For unidirectional laminates, the best correlation is obtained with Tsai-Wu, Hashin, and quadric surfaces criteria. For symmetric balanced laminates, $[(\theta/\text{-}\ \theta)_3]_s$, maximum stress and maximum strain estimate increased

strength for $[3]_{12}$ and $[6]_{12}$, while the others estimate first a decrease, after that continuous increase up to 45°. The experiments support the latter predicted trend. Hashin criterion shows the best correlation in general for symmetric balanced laminates. But for low-angle configurations like $[0_{12}]$ and $[(5/\text{-}5)_3]_s$, quadric surfaces criterion performs better for either unidirectional or symmetric-balanced configurations.

This study can be extended by using different AE methods. In this way, a progressive failure envelope can be drawn. Additionally, source location technique can be used to locate where failure starts.

APPENDIX A: ACOUSTIC EMISSION MONITORING

Acoustic Emissions are stress waves released by the structure caused by the micro-changes inside it. The raw emission are processed by an Acoustic Emission System as seen in the Figure A.1.

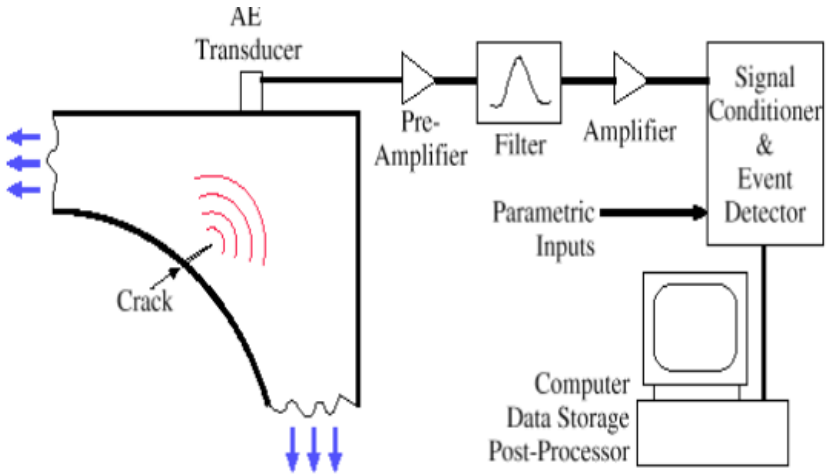

Figure A.1. An acoustic emission process system set up [37].

Acoustic emission (AE) systems are widely used in real time monitoring of composite materials. So, damage can be detected in-service. Since composite materials can fail with very different mechanisms, determining the governing failure mechanism is crucial for designers. AE systems present a very powerful tool for designers to get a knowledge about the inner state of the structure under loading.

The system used in this study is MISTRAS USB-AE NODE SYSTEM.

System consists of Piezoelectric Transducers and AE Node system.

Piezoelectric Transducers ; System include two piezolelectric transducers, PK15I, provided by Physical Acoustics Corporation (PAC). The goal of these sensors is catching acoustic signals, pre-amplify this signal and convey to the AE nodes.

AE Node System; Postprocesses and convert the features of the acquired data.

AE system needs some parameters to be given to acquire signal data. Some most important parameters are given below;

Peak definition Time (PDT); This parameter helps to ensure the time of true peak of the AE waveform [38]. PDT should be set as low as possible but it should be noted that setting PDT too low may cause false rise time measurements.

Hit definition Time (HDT); HDT enables the system to determine the end of the signal. This should be set minimum two times of PDT [31]. If HDT is set too high, it is possible to record two or more different events under one hit. On the contrary, if it is set too low, the software may divide one event into multiple hits [43].

Hit Lockout Time (HLT) ; The function of this parameter is to inhibit the measurement of reflections and late arriving parts of AE signal.

These timing parameters can be seen on the typical waveform in Figure A.2.

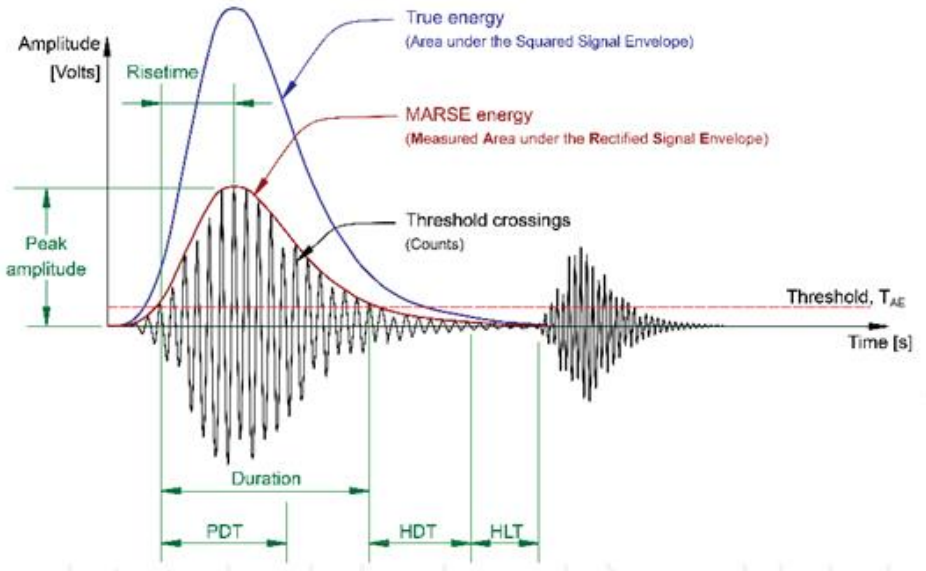

Figure A.2. A Typical Waveform [44].

Threshold; AE sensors are very sensitive so they are prone to process all sounds they catch.But using threshold, we eliminate the sounds of which amplitude below that limiting value.

Sample Rate; This is the rate at which the data acquisition board sample the waveform on per second basis. A sample rate on 1 MSPS (Mega Samples per Second) means that 1 waveform sample is taken in every micro seconds. [38]

The PDT, HDT and HLT values for different type of materials recommended by the MISTRAS Acoustic Emission Systems' Manual are seen on Table A.1.

Table A.1. Timing parameters recommended by MISTRAS [38].

	PDT	HDT	HLT
Composites,non metals	20- 50	100-200	300
Small metal specimens	300	600	1000
Metal Structures(High Damping)	300	600	1000
Metal Structures(Low Damping)	1000	2000	20000

REFERENCES

1. Cuadra J., *Damage Quantification in Fiber Reinforced Polymer Composites Using a Hybrid Non-Destructive Testing Approach*, M.S. Thesis, Drexel University, 2012.

2. Hyer, M., W., Stress Analysis of Fiber-Reinforced Composite Materials, McGraw-Hill, Michigan, 1998.

3. Jones, R., M., *Mechanics of Composite Materials,* 2nd Edition, Philadelphia, Taylor & Francis Inc., 1999.

4. Hill, R., *A Theory of Yielding and Plastic Flow of Anisotropic Metals,* Proceedings of the Royal Society Series A, London, 1948.

5. Hill, R., *The Mathematical Theory of Plasticity.* London : Oxford University Press, 1950.

6. Hashin, Z., "Failure Criteria for Unidirectional Fiber Composites", *Journal of Applied Mechanics,* Vol. 47, pp. 329-334, 1980.

7. Hoffman, O., "The Brittle Strength of Orthotropic Materials", *Journal of Composite Materials*, Vol.1, pp. 200-206, 1967.

8. Yeh, H., L., "Quadric Surfaces Failure Criterion for Composite Materials", *Journal of Reinforced Plastics and Composites,* Vol. 6., 2003.

9. Norris, C., B., "Strength of Orthotropic Materials Subjected to Combined Stress", *Forest Products Laboratory,* Report 1816, 1962.

10. Fischer, L., "Optimization of Orthotropic Laminates", *Journal of Engineering for Industry*, 1967.

11. Chamis, C., C., “Failure Criteria for Filamentary Composites”, Composite Materials: Testing and Design. ASTM STP 460, 1969.

12. Tsai, S., W., E., M., Wu, “A General Theory of Strength for Anisotropic Materials”, *Journal of Composite Materials*, Vol.5, pp. 58-80, 1971.

13. Puck, A., “A Failure Criteria Shows the Direction”, *Kunststoffe: German Plastics*, Vol. 82, pp. 29-32, 1992.

14. William E., S., Tarunjit, ’’A strain energy based failure criterion for non-linear analysis of composite laminates subjected to biaxial loading’’,*Failure Criteria in Fibre Reinforced Composite Materials,2004.*

15. Soden, P., D., M., J., Hinton, A., S., Kaddour, “A Comparison of the Predictive Capabilities of Current Failure Theories for Composite Laminates”, *Composite Science and Technology*, Vol. 58, pp. 1225-1254, 1998.

16. Soden, P., D., M., J., Hinton, “Predicting Failure in Composite Laminates: The Background to Exercise”, *Composite Science and Technology*, Vol. 58, 1998.

17. Kaddour, A., S., P., D., Soden and M., J., Hinton, **“**Biaxial Test Results for Strength and Deformation of a Range of E-Glass and Carbon Fiber Reinforced Composite Laminates: Failure Exercise Benchmark Data”, *Composite Science and Technology***.,** Vol. 62, pp. 1489-1514, 2002.

18. Puck and Schurrman., “Failure Analysis of FRP Laminates by Means of Physically Based Phenomenological Models”, *Composites Science and Technology*, Vol. 58, pp. 1045-1067, 2002.

19. Hinton, M., J., P., D., Soden and A., S., Kaddour, “A Comparison of the Predictive Capabilities of Current Failure Theories for Composite Laminates, Judged Aganist Experimental Evidence”, *Composite Science and Technology*, pp. 1725-1797, 2002.

20. Hara, E., T., Yokozeki, H., Hatta, H., Iwahori, T., Ogasawara, T., Ishikawa, " Comparison of out-of-plane tensile strengths of aligned CFRP obtained by 3-point bending and direct loading tests ", *Composites; Part A*, vol. 43, pp.1828-1836, 2012.

21. Feraboli ,P., K., T., Kedward, ''Four-point bend interlaminar shear testing of uni- and multi-directional carbon/epoxy composite systems'',*Composites:Part A:Applied Science and Manufacturing*, Vol.34 , pp. 1265,1271,2003.

22. Farshad, M., M., W., Wildenberg and P., Fluèeler, '' Determination of shear modulus and Poisson's ratio of polymers and foams by the anticlastic plate-bending method'', *Materials and Structures,*Vol. 30, pp. 377-382,1997.

23. Farshad, M. and P. Fluèeler, '' Investıgatıon of Mode III Fracture Toughness Usıng an Antİ-Clastıc Plate Bendıng Method'', *Engineering Fracture Mechanics*, Vol. 60, pp. 597-603,1998.

24. Podczeck, F., '' The determination of fracture mechanics properties of pharmaceutical materials in mode III loading using an anti-clastic plate bending method '', *International Journal of Pharmaceutics ,* Vol. 227, pp. 39-46,2001.

25. Gong, X., L., A., Laksimi, and M. L., Benzeghagh, "*Nouvelle Approche de L'émission Acoustique et son Application à L'identification des Mécanismes D'endommagement dans les Matériaux Composites*", Revue Des Composites et des Matériaux Avancés, Vol. 8, pp. 179-205, 1998.

26. Nimdum, P., J., Renard, "*Use of Acoustic Emission to Discriminate Damage Modes in Composite-Antenna Structure During Buckling Loading*", 15th International Conference on Experimental Mechanics, July,2012 .

27. De Groot, P., J., P., A., M., Wijnen, R., B., F., Jansen, "*Real-time frequency determination of acoustic emission for different fracture mechanisms in Carbon/Epoxy composites*", Composites Science and Technology, vol. 55, p. 405-412, 1995.

28. Giordano M., Calabro A., Esposito C., *D'Amore* Nicolais L., "An Acoustic Emission Characterisation of Failure Modes in Polymer-Composite Materials", Composites Science and Technology, vol. 58, p. 1923-1928, 1998.

29. Kam T., Y., F.,M., Lai, "Experimental and Theoretical Predictions of First Ply Failure Strength of Laminated Composite Plates", *International Journal of Solids and Structures,* vol. 36, p. 2379-2395, 1999.

30. Kam T., Y., Y., W., Liu, F.,T. Lee, "First Ply Strength of Laminated Composite Pressure Vessels", *Composite Structures,* vol. 38, p. 65-70, 1997.

31. Cure cycle, http://www.hexcel.com/Resources/DataSheets/Prepreg-Data Sheets/ 8552 _us.pdf, [Accessed August 2012].

32. Clarkson, E., "Hexcel 8552 AS4 Unidirectional Prepreg Qualification Statistical Report", *Natıonal Instıtute For Avıatıon Research*, Wichita State University.

33. ANSYS Help System, Version 13.0, 2010.

34. Koç M., F. O. Sonmez, "Failure Behavior Of Composıte Laminates Under Out-Of-Plane Loads" , Msc Thesis,Bogazici University, 2012.

35. Out of Autoclave Manufacturing Processes, http://en.wikipedia.org/wiki/ Out_of autoclavecomposite_manufacturing#Autoclave_curing_process_.28for_comparison_ purposes.29, [Accesed August 2014].

36. *Standard Test Method for Tensile Properties of Polymer Matrix Composite Materials*, ASTM International.

37. Mohd. S., "Acoustic Emission For Fatigue Crack Monitoring In Nuclear Piping System", Ph.D thesis, 2012.

38. USB AE Node™ & AEWIN™ For USB™ Software, User's Manual, January 2010.

39. AE signal processing https://www.ndeed.org/EducationResources/ Community College /Other%20Methods/AE/AE_Signal%20Features.htm [Accesed 2014].

40. Noorsuhada M., D., A., Ibrahim, "Relationship between acoustic emission signal strength and damage evaluation of reinforced concrete structure: Case studies", 2011 IEEE Symposium on Industrial Electronics and Applications, 2011.

41. Rao A., D., "Acoustic Emissions and Signal Analysis", *Defence Science Journal*, vol.40, pp. 55-70, 1990.

42. Gutkin R., C., J., Grenn, S., Vangrattanachai, S., T., Pinho, P., Robinson, P., T., Curtis, "On acoustic emission for failure investigation in CFRP: Pattern recognition and peak frequency analyses", *Mechanical Systems and Signal Processing*, vol. 25, pp. 1393-1407, 2011.

43. Barsoum, F., F., J., Suleman, A., Korcak, and E., V., K., Hill, "Acoustic Emission Monitoring and Fatigue Life Prediction in Axially Loaded Notched Steel Specimens", *Journal of Acoustic Emission*, Vol. 27, pp. 40-63, 2009.

44. Unnþórsson, R., "Hit Detection and Determination in AE Bursts, Acoustic Emission - Research and Applications", 2013, http://www.intechopen.com/books/acousticemission-research-and-applications/hit-detection-and-determination-in-ae-burst, [Accessed August 2014].